

1 **Cell – ECM interactions play distinct and essential roles at multiple stages during**  
2 **the development of the aortic arch**

3  
4 Michael Warkala<sup>1,2, §</sup>, Dongying Chen<sup>3, §, ¥</sup>, Ali Jubran<sup>3, †</sup>, AnnJosette Ramirez<sup>1,4, †</sup>,  
5 Michael Schonning<sup>1,4</sup>, Xia Wang<sup>†</sup>, Huaning Zhao<sup>1</sup>, and Sophie Astrof<sup>1, 2, 4, \*</sup>.

6  
7 1. Department of Cell Biology and Molecular Medicine, New Jersey Medical School,  
8 Rutgers Biomedical and Health Sciences, Newark, NJ, USA

9  
10 2. Multidisciplinary Ph.D. Program in Biomedical Sciences: Molecular Biology, Genetics,  
11 and Cancer Track, New Jersey Medical School, Rutgers Biomedical and Health  
12 Sciences, Newark, NJ, USA

13  
14 3. Graduate Program in Cell & Developmental Biology, Thomas Jefferson University,  
15 Philadelphia, PA, USA

16  
17 4. Multidisciplinary Ph.D. Program in Biomedical Sciences: Cell Biology, Neuroscience  
18 and Physiology Track, New Jersey Medical School, Rutgers Biomedical and Health  
19 Sciences, Newark, NJ, USA

20  
21 ¥ Current address: Yale Cardiovascular Research Center, Department of Internal  
22 Medicine, Yale University School of Medicine, New Haven, CT 06511, USA.

23

24 ‡ Current address: Department of Anatomy, Histology & Developmental Biology, School  
25 of Basic Medical Sciences, Shenzhen University Health Science Center, Shenzhen,  
26 China

27

28 § These individuals contributed equally to the manuscript as co-first authors

29 † These individuals contributed equally to the manuscript as co-second authors

30

31 Short title: Integrin  $\alpha 5\beta 1$  and Fn1 in arch artery formation

32

33 \* Corresponding author: Sophie Astrof,

34 [sophie.astrof@rutgers.edu](mailto:sophie.astrof@rutgers.edu)

35

36

37 185 South Orange Ave,

38 Medical Sciences Building, Room I-518,

39 Newark, NJ, 01703

40

41 Total word count: 7746

42 Subject Codes: Animal Models of Human Disease; Mechanisms; Vascular Biology;

43 **Rationale:** Defects in the morphogenesis of the 4<sup>th</sup> pharyngeal arch arteries (PAAs)  
44 give rise to lethal birth defects. Understanding genes and mechanisms regulating PAA  
45 formation will provide important insights into the etiology and treatments for congenital  
46 heart disease.

47 **Objective:** Cell-ECM interactions play essential roles in the morphogenesis of PAAs  
48 and their derivatives, the aortic arch artery (AAA) and its major branches; however, their  
49 specific functions are not well-understood. Previously, we demonstrated that integrin  
50  $\alpha 5\beta 1$  and fibronectin (Fn1) expressed in the *Isl1* lineages regulate PAA formation. The  
51 objective of these studies was to investigate cellular mechanisms by which integrin  
52  $\alpha 5\beta 1$  and Fn1 regulate AAA morphogenesis.

53 **Methods and Results:** Using temporal lineage tracing, whole-mount confocal imaging,  
54 and quantitative analysis of the second heart field (SHF) and endothelial cell (EC)  
55 dynamics, we show that the majority of PAA EC progenitors arise by E7.5 in the SHF  
56 and populate pharyngeal arch mesenchyme between E7.5 and E9.5. Consequently,  
57 SHF-derived ECs in the pharyngeal arches become organized into a uniform plexus of  
58 small blood vessels, which becomes remodeled into the PAAs between 31 – 35  
59 somites. The remodeling of the vascular plexus is orchestrated by signals dependent on  
60 pharyngeal ECM microenvironment extrinsic to the endothelium. Conditional ablation of  
61 integrin  $\alpha 5\beta 1$  or Fn1 in the *Isl1* lineages showed that signaling by the ECM regulates  
62 AAA morphogenesis at multiple steps: 1) the recruitment of the SHF-derived ECs into  
63 the pharyngeal arches, 2) the remodeling of the uniform EC plexus in the 4<sup>th</sup> arches into  
64 the PAAs; and 3) differentiation of neural crest-derived cells abutting the PAA  
65 endothelium into vascular smooth muscle cells.

66 **Conclusions:** PAA formation is a multi-step process entailing dynamic contribution of  
67 SHF-derived ECs to pharyngeal arches, the remodeling of endothelial plexus into the  
68 PAAs, and the remodeling of the PAAs into the AAA and its major branches. Cell-ECM  
69 interactions regulated by integrin  $\alpha 5\beta 1$  and Fn1 play essential roles at each of these  
70 developmental stages.

71 Key Words: integrin  $\alpha 5\beta 1$ , fibronectin, second heart field, endothelial progenitor cells,  
72 pharyngeal arch arteries, aortic arch arteries

73 **Nonstandard Abbreviations and Acronyms in the Alphabetical Order:** AAA – aortic  
74 arch artery; CHD – congenital heart disease; ECs – endothelial cells; Fn1 – fibronectin;  
75 IAA-B – interrupted aortic arch type B; Itga5 – integrin  $\alpha 5$ ; PAA – pharyngeal arch  
76 arteries; RERSA – retro-esophageal right subclavian artery; SHF – second heart field;  
77 VEGFR2 – vascular endothelial growth factor receptor 2

78

## 79 **Introduction**

80 Aortic arch artery (AAA) and its major branches comprise an asymmetrical vascular tree  
81 that routes oxygenated blood from the heart into the systemic circulation <sup>1</sup>. Defects in  
82 the development of the AAA cause devastating forms of congenital heart disease (CHD)  
83 due to interruption(s) in the aortic arch, of which interrupted aortic arch type B (IAA-B) is  
84 more prevalent <sup>2, 3</sup>. Non-lethal defects in aortic arch morphogenesis such as vascular  
85 rings can impact the quality of life by causing constriction of the trachea and esophagus,  
86 and resulting in difficulties with eating, breathing, and also in dizziness, vertigo, or  
87 tinnitus <sup>4</sup>.

88         The AAA and its major branches develop from the remodeling of three bilaterally  
89 symmetrical pairs of pharyngeal arch arteries (PAA), numbered 3, 4, and 6 <sup>5</sup>. It is  
90 important to note that phenotypically identical AAA defects arise due to either defects in  
91 PAA formation or defects in the remodeling of initially well-formed, symmetrical PAAs  
92 into asymmetric AAAs <sup>6</sup>. PAAs arise by vasculogenesis from endothelial precursors  
93 originating in the lateral plate mesoderm, also known as the second heart field (SHF) <sup>7-</sup>  
94 <sup>13</sup>. Experiments in zebrafish and mice have demonstrated that PAA formation is a multi-  
95 stage process that entails endothelial specification in the SHF, migration of SHF-derived  
96 endothelial progenitors into the pharyngeal region, differentiation into ECs, and the  
97 assembly of SHF-derived ECs into a plexus of small blood vessels <sup>9, 13-16</sup>. Thereafter,  
98 the pharyngeal endothelial plexus becomes connected with the ventral and dorsal  
99 aortae. The endothelium of the ventral aortae also forms by vasculogenesis from SHF-  
100 derived progenitors and is contiguous with the cardiac outflow tract and the PAAs <sup>9, 11</sup>.  
101 Following pharyngeal arch segmentation, the plexus endothelium within each arch is

102 rearranged into the PAAs<sup>9</sup>. The 3<sup>rd</sup> PAA is evident by E9.5, before the 4<sup>th</sup> and 6<sup>th</sup> PAAs  
103 are formed. By the evening of E10.5, all three symmetrical pairs of PAAs are formed.  
104 Defects in the formation of the left 4<sup>th</sup> PAA lead to IAA-B, which is lethal unless  
105 corrected by surgery soon after birth<sup>2</sup>. Following PAA formation, neural crest-derived  
106 cells closest to the PAA endothelium differentiate into vascular smooth muscle cells  
107 (VSMCs), surrounding the PAA endothelium with a VSMC coat by E12.5<sup>17-21</sup>. While not  
108 essential for PAA formation, the differentiation of neural crest (NC)-derived cells into  
109 VSMCs is essential for the stability of the PAAs, and for their eventual remodeling into  
110 the asymmetrical AAA and its branches; Defects in NC differentiation in the 4<sup>th</sup>  
111 pharyngeal arch lead to arch artery regression, and IAA-B<sup>19, 20, 22</sup>. In summary, IAA-B  
112 results due to either defects in the formation of the left 4<sup>th</sup> PAA or due to its regression.

113 Morphogenesis of distinct organs and structures proceeds within niches  
114 comprised of distinct complements of extracellular matrix (ECM) proteins, and  
115 alterations in ECM microenvironment can severely affect embryogenesis<sup>23-27</sup>. We  
116 discovered that the pharyngeal arch microenvironment is enriched in the ECM  
117 glycoprotein fibronectin (Fn1) both at the mRNA and protein levels<sup>28</sup>. Fn1 is highly  
118 expressed in the pharyngeal endoderm, ectoderm, endothelium, and the second heart  
119 field (SHF) mesoderm between E8.5 and E10.5, the period coinciding with PA formation  
120<sup>28, 29</sup>. Between E10.5 and E11.5 Fn1 becomes highly upregulated in the NC-derived  
121 cells abutting the 4<sup>th</sup> PAA endothelium, corresponding with the time these cells  
122 differentiate into VSMCs. Our previous studies demonstrated that local depletion of Fn1  
123 in the pharyngeal microenvironment using the *Isl1*<sup>Cre</sup> knockin mice or in the NC-derived  
124 cells, using a variety of NC-expressing Cre lines, resulted in the IAA-B and RERSA<sup>29</sup>,

125 <sup>30</sup>. However, mechanistically, IAA-B in these mutants had distinct cellular etiology:  
126 ablation of Fn1 in using the *Isl1<sup>Cre</sup>* knockin mice led to defective formation of the 4<sup>th</sup>  
127 PAAs <sup>29</sup>, while the ablation of Fn1 in the NC resulted in the regression of originally well-  
128 formed 4<sup>th</sup> PAAs <sup>31</sup>.

129 Integrins are a major class of transmembrane receptors that engage in signal  
130 transduction upon binding ECM proteins. Integrins are heterodimers of  $\alpha$  and  $\beta$  chains.  
131 There are 18  $\alpha$  and 8  $\beta$  subunits encoded by mammalian genomes, giving rise to 24  
132 different  $\alpha\beta$  combinations <sup>32</sup>. Integrin  $\alpha5$  complexes with integrin  $\beta1$ , forming the integrin  
133  $\alpha5\beta1$  heterodimer <sup>33</sup>. Integrin  $\alpha5\beta1$  binds the ECM glycoprotein fibronectin (Fn1), and  
134 regulates Fn1 assembly *in vivo* <sup>34</sup>. Phenotypes resulting from either global or cell-type-  
135 specific ablations of integrin  $\alpha5$  (MGI gene symbol: *Itga5*) or Fn1 in mice are similar <sup>26</sup>,  
136 <sup>28, 29, 31, 34-41</sup>, indicating that integrin  $\alpha5\beta1$  is a major Fn1 signal transducer *in vivo*.  
137 Previously, we demonstrated that the expression of integrin  $\alpha5\beta1$  and Fn1 in the *Isl1*  
138 lineages was required for the formation of the 4<sup>th</sup> PAA and that the deletion of either  
139 integrin  $\alpha5$  or Fn1 in using the *Isl1<sup>Cre</sup>* knockin strain resulted in IAA-B <sup>29</sup>. To understand  
140 the mechanisms by which integrin  $\alpha5\beta1$  and Fn1 regulate AAA development, we  
141 analyzed SHF and endothelial cell dynamics in integrin  $\alpha5^{f/-}$ ; *Isl1<sup>Cre</sup>* and *Fn1<sup>f/-</sup>*; *Isl1<sup>Cre</sup>*  
142 mutants during PAA formation and remodeling, spanning embryonic days (E) E9.5 -  
143 E11.5 of development. Our studies point to the essential roles of cell-ECM interactions  
144 mediated by integrin  $\alpha5\beta1$  and Fn1 at multiple stages of PAA formation and remodeling.

145

146 **Methods**

147 **Animals** All experimental procedures were approved by the Institutional Animal Care  
148 and Use Committee of Rutgers University and conducted in accordance with the  
149 Federal guidelines for the humane care of animals.

150 **Tamoxifen injections** *Isl1<sup>MerCreMer</sup>* knockin mice <sup>42</sup> and *Mef2C-AHF-DreERT2*  
151 transgenic mice <sup>43</sup> were used for temporal labeling of vascular progenitors in the SHF.  
152 Tamoxifen was dissolved either in corn oil or in sesame oil at the concentration of 10  
153 mg/ml. Labeling was done by i.p. injection of 300  $\mu$ l of stock solution into pregnant  
154 females at multiple time points specified in the legend to Fig. 1. E0.5 was designated to  
155 be as noon on the day when the vaginal plug was found.

156 **Whole Mount Immunofluorescence staining** Labeling with BrdU, TUNEL, and  
157 staining with antibodies were performed as described <sup>29</sup>, and analyzed using IMARIS  
158 (Bitplane, USA) <sup>9, 44</sup>. Detailed procedures for staining, analysis and cell quantification is  
159 described in <sup>44</sup>.

160

161 **Statistics** Statistical analyses were performed using Prism 8 software version 8.4.3.  
162 Specific statistical tests are indicated in figure legends.

163

## 164 **Results**

165 **SHF contributes harbors PAA progenitors between E7.5 and E9.5.** Previous work  
166 from our lab demonstrated that in the mouse, the majority of PAA endothelium is  
167 derived from the SHF, derived from either *Mef2C-AHF-Cre-* or *Isl1<sup>Cre-</sup>* expressing  
168 mesodermal lineages <sup>9</sup>. To define the temporal window during which the SHF



169 mesoderm harbors endothelial progenitors of the PAAs, we used *Isl1<sup>MerCreMer</sup>* knockin  
170 mice <sup>42</sup> and Mef2C-AHF-DreERT2 transgenic mice <sup>43</sup> combined with pulses of tamoxifen  
171 to lineage-label the SHF mesoderm at different developmental times (Fig. 1). Tamoxifen  
172 was injected at discrete time points between E6.75 – E9.75, and embryos were  
173 dissected at E10.5 and stained to detect lineage labeling in the pharyngeal arches.  
174 Entire pharyngeal regions were imaged using confocal microscopy to quantify the  
175 contribution of lineage-labeled cells to the PAA endothelium (Fig. 1, panels A-A2). The  
176 expression of VEGFR2 and ERG were used to mark EC cell membrane and nuclei <sup>45</sup>.  
177 The labeling of the cardiac outflow tract and the right ventricle using *Isl1<sup>MerCreMer</sup> / +* mice  
178 was evident at all stages tested, indicating that our labeling technique was consistent  
179 with previous studies (data not shown) <sup>42</sup>. Myocardial cells derived from the SHF are  
180 labeled when tamoxifen is injected as early as E6.5 in *Isl1<sup>MerCreMer</sup>* knockin mice <sup>42</sup>,  
181 however no PAA ECs were labeled when tamoxifen was injected at E6.75 in this strain  
182 (Fig. 1B) or at E7.25 in Mef2C-AHF-DreERT2 transgenic strain (Fig. 1C), suggesting  
183 that PAA EC progenitors arise later in the SHF relative to cardiomyocyte progenitors.  
184 The peak labeling of the PAA endothelium occurred when tamoxifen was injected at  
185 E7.25 in *Isl1<sup>MerCreMer</sup>* strain (Fig. 1B) and at E8.0 in Mef2C-AHF-DreERT2 strain (Fig.  
186 1C). While tamoxifen injection into *Isl1<sup>MerCreMer</sup>* resulted in sparse labeling of PAA ECs,  
187 the injection of tamoxifen into Mef2C-AHF-DreERT2 transgenic mice led to the labeling  
188 of a much larger proportion of ECs in the PAAs (compare Fig. 1B with Fig. 1C). These  
189 differences likely reflect that the MerCreMer transgene is present as a single copy as it  
190 is knocked into the *Isl1* locus <sup>42</sup>, while Mef2C-AHF-DreERT2 is a transgenic strain  
191 containing multiple copies of the Mef2C-AHF-DreERT2 transgene <sup>43</sup>. In addition, the

192 expression of *Isl1* is downregulated commensurate with endothelial differentiation <sup>46</sup>.  
193 Thus, potentially low levels of *MerCreMer* expression in EC precursors could have  
194 resulted in low labeling of endothelial progenitors in *Isl1<sup>MerCreMer</sup>* mice relative to Mef2C-  
195 AHF-DreERT2 strain. The difference in the timing of peak EC labeling in the PAAs  
196 between *Isl1<sup>MerCreMer</sup>* and Mef2C-AHF-DreERT2 strains is likely due to the earlier onset  
197 of *Isl1* expression compared with the expression of the Mef2C-AHF-DreERT2  
198 transgene; in fact, *Isl1* regulates the expression of Mef2C and the activation of the  
199 Mef2C-AHF enhancer <sup>47, 48</sup>. Correspondingly, our experiments demonstrate that the  
200 peak endothelial labeling of PAAs in *Isl1<sup>MerCreMer</sup>* strain precedes that of Mef2C-Dre-  
201 ERT2 strain by 18 hours (compare Fig. 1B with Fig. 1C). Interestingly, the accrual of  
202 SHF-derived ECs into the 4<sup>th</sup> arch continues past E8.5 as more SHF-derived cells are  
203 labeled in the 4<sup>th</sup> PAAs than in the 3<sup>rd</sup> and 6<sup>th</sup> when tamoxifen is injected at E8.5 and  
204 E9.5 (Fig. 1B1, 1C1). Thus, our labeling experiments show that the SHF mesoderm  
205 harbors PAA endothelial progenitors between approximately E7.5 and E9.5 of  
206 embryonic development.  
207  
208 To analyze the contribution of the SHF to the PAA endothelium quantitatively and to  
209 compare two mouse strains commonly used to label the SHF, we imaged the entire  
210 pharyngeal arch region corresponding to arches 3, 4, and 6, and quantified the  
211 proportion of SHF-lineage labeled ECs in the PAAs from E10.5 embryos derived from  
212 *Isl1<sup>Cre</sup>* knockin and Mef2C-AHF-Cre transgenic lines (Fig. 2). The majority of SHF-  
213 derived cells in the pharyngeal arches 3 – 6 are found in the endothelium at 37somites,  
214 as seen in sections through the pharyngeal arch region (Fig. 2A – B). Each PAA is

215 comprised of a similar number of ECs (Fig. 2C). However, there were differences in  
216 PAA labeling among embryos isolated from *Isl1<sup>Cre</sup>* and *Mef2C-AHF-Cre* mice (Fig. 2D,  
217 E). In the constitutive *Isl1<sup>Cre</sup>* knockin strain, the SHF contribution to the 3<sup>rd</sup> and 4<sup>th</sup> PAA  
218 endothelium was 79±6% and 77±10%, respectively, and 57±12% to the 6<sup>th</sup> PAA (Fig.  
219 2D). While the SHF contribution to the 3<sup>rd</sup> PAA was 45±8% in *Mef2C-AHF-Cre*  
220 transgenic line, which is significantly different from *Isl1<sup>Cre</sup>* knockin strain ( $p < 10^{-5}$ , one-  
221 way ANOVA with Tukey's correction for multiple testing). The SHF contribution to the  
222 PAA endothelium of the 4<sup>th</sup> and 6<sup>th</sup> PAAs were similar between the two strains ( $p > 0.2$ ,  
223 one-way ANOVA with Tukey's correction for multiple testing). The difference in the  
224 contribution of the SHF to the 3<sup>rd</sup> PAA between the two strains likely reflects the earlier  
225 onset of Cre expression in the *Isl1<sup>Cre</sup>* knockin strain relative to *Mef2C-AHF-Cre*  
226 transgenic line<sup>47</sup>. These data suggest that about half of the 3<sup>rd</sup> PAA progenitors arise  
227 and leave the SHF prior to the activation of *Mef2C-AHF-Cre*. These data also indicate  
228 that the deletion of one *Isl1* allele, as in the *Isl1<sup>Cre</sup>* knockin strain, does not impair the  
229 contribution of the SHF to the PAA endothelium. In summary, our data show that the 4<sup>th</sup>  
230 PAAs differ from the 3<sup>rd</sup> and the 6<sup>th</sup> PAAs in the timing during which SHF cells are  
231 added, and differ from the 6<sup>th</sup> PAA in the proportion of SHF-derived cells.

232

233 **Cell-ECM interactions mediated by integrin  $\alpha 5\beta 1$  specifically regulate the accrual**  
234 **of SHF-derived cells into pharyngeal region.** Studies described above together with  
235 our previous work<sup>9</sup> have established a framework for the analyses of EC dynamics and  
236 their genetic regulation during the morphogenesis of AAA and its major branches. Our  
237 previous studies demonstrated that the deletion of either integrin  $\alpha 5$  or *Fn1* in the *Isl1*

238 lineages resulted in the defective formation of the 4<sup>th</sup> PAAs at E10.5, and consequently,  
239 IAA-B and retro-esophageal right subclavian artery (RERSA), in these mutants<sup>29</sup>. IAA-B  
240 and RERSA are anomalies resulting from defective morphogenesis of the left and right  
241 4<sup>th</sup> PAAs, respectively<sup>1,3</sup>. To determine the mechanisms by which integrin  $\alpha 5\beta 1$  and  
242 Fn1 regulate the formation of the 4<sup>th</sup> PAAs, we analyzed PAA development at distinct  
243 stages of embryonic development using whole-mount immunofluorescence followed by  
244 quantitative analyses of SHF-derived populations and their dynamics.

245  
246 PAAs form through the coalescence of pharyngeal arch EC plexus, a network of small  
247 blood vessels<sup>9,10</sup>. All pharyngeal arch ECs are located within the plexus at E9.5. At  
248 E10.5 (33 – 34 somite stage), 50% of the 4<sup>th</sup> arch endothelium is found within the PAA  
249 (the vessel surfaced in green in (Fig. 3B, C) and 50% is in the plexus (pink in Fig. 3B, C)  
250<sup>9</sup>. About 50% of integrin  $\alpha 5^{fl/-}; Isl1^{Cre}$  mutants have defective 4<sup>th</sup> PAAs, and  
251 consequently, 50% of these mutants develop IAA-B and RERSA<sup>29</sup>. We found that 4<sup>th</sup>  
252 PAA is absent in 50% of mutants at 32 – 34 somites (Fig. 3D – F). Instead, the  
253 endothelium in the 4<sup>th</sup> arches is in the form of a plexus of small blood vessels (marked  
254 in pink in Fig. 3E, F). A small 4<sup>th</sup> PAA eventually formed in these mutants by 36 – 39  
255 somites (Fig. 3J, marked in green in Fig. 3K, L; compare with the 4<sup>th</sup> PAA surfaced in  
256 green in control Fig. 3G-I). Similarly, the formation of the 4<sup>th</sup> PAA was delayed in  $Fn1^{fl/-};$   
257  $Isl1^{Cre/+}$  mutants (Sup. Fig. 1). This defect was specific to the 4<sup>th</sup> PAA, as the 3<sup>rd</sup> and 6<sup>th</sup>  
258 PAAs formed normally in the mutants (vessels surfaced in white and red in Fig. 3). The  
259 incidence of IAA-B and RERSA is 50% in integrin  $\alpha 5^{fl/-}; Isl1^{Cre}$  and  $Fn1^{fl/-}; Isl1^{Cre/+}$   
260 mutants, which is the same as the incidence of defective 4<sup>th</sup> PAAs at E10.5<sup>29</sup>.

261 Therefore, we further investigated the mechanisms by which integrin  $\alpha 5\beta 1$  and Fn1  
262 regulate the formation of the 4<sup>th</sup> PAAs.

263 We hypothesized that the defective formation of the 4<sup>th</sup> PAAs in our mutants could be  
264 due to insufficient EC numbers, defective EC proliferation, or survival. To test these  
265 hypotheses, we evaluated total EC numbers in the 4<sup>th</sup> pharyngeal arches of controls  
266 and mutants. To quantify EC number, we stained E10.5 embryos with the antibodies to  
267 ERG, a transcription factor enriched in the endothelia and either VEGFR2 or Pecam 1,  
268 expressed on EC surface, as described<sup>44</sup>. These experiments showed that integrin  $\alpha 5^{f/-}$   
269 ;  $Isl1^{Cre}$  and  $Fn1^{f/-}$ ;  $Isl1^{Cre/+}$  mutants had decreased total number of ECs in the 4<sup>th</sup> arches  
270 at 32 – 33 somites relative to controls (Fig. 3M and Sup. Fig. 1A-C). Despite this  
271 decrease in EC numbers, the size of the 4<sup>th</sup> arches, the tissues within which PAAs form,  
272 was not affected (Fig. 3N). EC proliferation in the 4<sup>th</sup> arch was also not affected in the  
273 mutants (Fig. 3O), and neither was cell survival (Sup. Fig. 2). Thus, EC deficiency in the  
274 4<sup>th</sup> pharyngeal arches of the mutants was not due to defective cell proliferation or  
275 survival. The majority of VEGFR2<sup>+</sup> cells in the pharyngeal region of E9.5 embryos were  
276 labeled with GFP (Sup. Fig. 3A – A2, B – B2), indicating that SHF cells in the  
277 pharyngeal region of the mutants were not impaired in the acquisition of EC fate.

278 VEGFR2 is expressed the 4<sup>th</sup> pharyngeal arch endothelium at E9.5, which is a day  
279 earlier than Pecam 1<sup>10</sup>. To determine whether the maturation of pharyngeal arch ECs  
280 was affected in the mutants at E10.5, we co-stained embryos with antibodies to  
281 VEGFR2 and Pecam 1. Despite defective 4<sup>th</sup> PAA formation, all VEGFR2<sup>+</sup> cells in  
282 pharyngeal arches of the mutants also expressed Pecam1 at E10.5 (Sup. Fig. 3C, D,

283 C1, D1), ruling out maturation as a cause for decreased EC numbers in the 4<sup>th</sup>  
284 pharyngeal arch.

285 Since the maturation, proliferation, and survival of ECs were not affected in our mutants,  
286 we tested the hypothesis that defective recruitment of progenitor cells into the  
287 pharyngeal arches was the cause for decreased EC numbers in the 4<sup>th</sup> arch. As we  
288 established before, the majority of PAA endothelium arises from the SHF (Fig. 2D, E  
289 and <sup>9</sup>, and the accrual of SHF-derived cells into the pharyngeal arches is mostly  
290 complete by E9.5 (Fig. 1B-C). To quantify the number of SHF-derived cells in the  
291 pharyngeal mesenchyme, we used ROSA<sup>nT-nG</sup> reporter mice, in which nuclear  
292 localization sequences were fused with tdTomato and EGFP, leading to the expression  
293 nuclear-localized EGFP upon Cre-induced recombination. We found that the deletion of  
294 integrin  $\alpha 5$  in the *Isl1* lineages impaired the accrual of SHF cells into the pharyngeal  
295 region (Fig. 4A-B), while the accrual of SHF-derived cells into the heart was not affected  
296 (Fig. 4C).

297

298 Splanchnic mesoderm within the dorsal pericardial wall harbors both cardiac and  
299 vascular progenitors. To test whether the deficiency in the pharyngeal SHF-derived  
300 mesoderm was due to the decrease in SHF cells numbers in the splanchnic mesoderm,  
301 we used IMARIS to surface cells within this region and quantified the number of GFP<sup>+</sup>  
302 cells (see Sup. Fig. 4 for details on surfacing). These experiments showed that the  
303 number of GFP<sup>+</sup> cells in the splanchnic mesoderm within the dorsal pericardial wall was  
304 similar between controls and mutants (Fig. 4D). Next, we computed the proportion of

305 GFP<sup>+</sup> cells in the pharyngeal mesenchyme or in the heart relative to the number of  
306 GFP<sup>+</sup> cells in the splanchnic mesoderm. While the latter ratio was not affected in the  
307 mutants (Fig. 4E), the former was significantly decreased in the mutants (Fig. 4F),  
308 suggesting that there is a defect either in the specification of pharyngeal progenitors in  
309 the SHF or in their exit from the SHF. Taken together, these experiments indicate that  
310 ECM microenvironment sensed through the signaling by integrin  $\alpha 5\beta 1$  is important for  
311 the accrual of the SHF-derived mesoderm to the pharyngeal arches (Model in Fig. 8,  
312 PAA formation panel A1).

313

314 **Integrin  $\alpha 5\beta 1$  and fibronectin regulate the remodeling of pharyngeal plexus into**  
315 **the 4<sup>th</sup> PAAs independently of EC numbers.** Interestingly, the number of SHF-derived  
316 cells and ECs in the mutants recovered by the 34-35 somite stage, and was similar to  
317 that of controls (Fig. 5A). Total number of GFP<sup>+</sup> cells also recovered (Fig. 5B). The  
318 percentage of GFP<sup>+</sup> ECs in the pharyngeal arches of controls and mutants were  
319 comparable (Fig. 5C), indicating that the recovery was not due to the recruitment of ECs  
320 from an alternative mesodermal source. The recovery of pharyngeal EC numbers was  
321 likely mediated through the proliferation of SHF-derived ECs. The basis for this  
322 conclusion is the following. The proliferation index of pharyngeal arch ECs was  
323 unaltered in the mutants (Fig. 3O), and the proliferation index of ECs in the pharyngeal  
324 plexus is 2-fold higher than that of PAA ECs, both in controls and in mutants (Fig. 3O,  
325 plexus). Since the proportion of ECs in the pharyngeal plexus is higher in the mutants  
326 than in controls (Sup. Fig 1D), the higher proliferation index of plexus ECs in the mutants  
327 is likely responsible for EC recovery. Our quantitative analyses indicate that PAA

328 formation phenotypes in integrin  $\alpha 5^{f/-}$ ;  $Isl1^{Cre/+}$  and  $Fn1^{f/-}$ ;  $Isl1^{Cre/+}$  mutants are  
329 indistinguishable from one another (Sup. Fig. 1), suggesting that integrin  $\alpha 5\beta 1$  is a  
330 major receptor transducing Fn1 signals within the pharyngeal microenvironment.

331 Despite the recovery of EC numbers (Fig. 5A), PAAs remained thin in integrin  $\alpha 5^{f/-}$ ;  
332  $Isl1^{Cre}$  and  $Fn1^{f/-}$ ;  $Isl1^{Cre/+}$  mutants (Fig. 3G – L), and there was 2 – 3-fold decrease in  
333 the proportion of pharyngeal arch ECs in the 4<sup>th</sup> PAAs at all stages analyzed at E10.5  
334 (Fig. 6A). The size of the 4<sup>th</sup> PAA increases between 32 – 39 somites, as more ECs are  
335 added to the PAA from the plexus (Sup. Fig. 5), and is reflected in the percent of  
336 pharyngeal arch ECs in the PAA<sup>9</sup>. In controls, plexus ECs in the 4<sup>th</sup> arch begin  
337 coalescing into the PAA when embryos reach between 31 and 32 somites<sup>9</sup> (Sup. Fig.  
338 5). These rearrangements result in an initially thin 4<sup>th</sup> PAAs, in which approximately  
339 50% of the pharyngeal arch ECs are in the plexus and 50% in the PAA at 32 – 34  
340 somite stage<sup>9</sup>. As the development proceeds, by 36-39 somite stage, > 60% of the 4<sup>th</sup>  
341 pharyngeal arch endothelium becomes incorporated into the 4<sup>th</sup> PAA<sup>9</sup>. Thus, the  
342 percentage of the pharyngeal arch endothelium in the 4<sup>th</sup> PAA can be taken as a  
343 measure of PAA formation. The higher the proportion, the larger the PAA<sup>9</sup>.

344 To understand the mechanisms by which integrin  $\alpha 5\beta 1$  and Fn1 regulate the  
345 remodeling of the uniform endothelial plexus into the PAA in the 4<sup>th</sup> arch, we examined  
346 EC dynamics in control and mutant embryos at three time points, corresponding with 32  
347 – 33 somites, 34 – 35 somites, and 36 – 39 somites. These stages span about 6 hours  
348 on the 10<sup>th</sup> day of mouse embryonic development. The formation of the 4<sup>th</sup> PAAs lagged  
349 in mutants relative to controls at all time points tested during E10.5 (Fig. 6A and Sup  
350 Fig. 1D, E), and 7 of the 16 embryos analyzed contained only a plexus of ECs and



351 lacked the 4<sup>th</sup> PAAs at the 32 – 34 somite stage (Sup. Fig. 1E), a stage at which over  
352 50% of the 4<sup>th</sup> arch endothelium in controls is located within the 4<sup>th</sup> PAAs<sup>9</sup> (Fig. 6A and  
353 Sup Fig. 1E).

354 Since mutant embryos had fewer ECs in the 4<sup>th</sup> pharyngeal arches compared with  
355 controls prior to the 36<sup>th</sup> somite stage, we performed correlation analyses to test the  
356 hypothesis that the formation of the 4<sup>th</sup> PAAs depended on the total EC number or EC  
357 density in the 4<sup>th</sup> pharyngeal arches. As described above, the percentage of pharyngeal  
358 arch ECs in the PAA relative to the plexus can be taken as a measure of PAA formation  
359 (Sup. Fig. 5)<sup>9</sup>. Thus, for these analyses, we quantified EC numbers in control embryos  
360 isolated between 32 to 39 somite stages and plotted them against the percent of ECs in  
361 the 4<sup>th</sup> PAAs (Fig. 6B). Despite the sharp, over a 3-fold increase in the number of ECs in  
362 the 4<sup>th</sup> arches between these stages<sup>9</sup>, the formation of the 4<sup>th</sup> PAAs was independent  
363 of the total EC number in the 4<sup>th</sup> pharyngeal arch tissue (Fig. 6B) or EC density (Fig.  
364 6C) in controls throughout the 10<sup>th</sup> day of embryonic development. Similarly, correlation  
365 analysis of PAA formation in the mutants with defective (thin) and normal 4<sup>th</sup> PAAs,  
366 showed that similar to controls, the rearrangement of plexus ECs into the PAA did not  
367 depend on the number of total number of ECs in the 4<sup>th</sup> pharyngeal arches of mutants  
368 (Fig. 6D).

369 Next, we compared PAA formation in controls and mutants that had a similar number of  
370 ECs in the 4<sup>th</sup> pharyngeal arches (Fig. 6E). These analyses showed that in groups of  
371 mutant and control embryos with a similar number of ECs, the percent of ECs in the  
372 PAAs was lower in the mutants (boxes in Fig. 6E). These data indicate that the  
373 reorganization of the plexus ECs into the PAA in the 4<sup>th</sup> pharyngeal arch does not

374 depend on the EC number at E10.5, and is regulated by factors extrinsic to the  
375 pharyngeal arch endothelium. In summary, our studies indicate that during the 10<sup>th</sup> day  
376 of embryonic development, cell – ECM interactions mediated by integrin  $\alpha 5\beta 1$  and Fn1  
377 are essential for the remodeling of the initially uniform vascular plexus into the PAA in  
378 the 4<sup>th</sup> pharyngeal arches (Model in Fig. 8, PAA formation panel A2).

379

380 **The expression of integrin  $\alpha 5$  in the *Isl1* lineage is required for the differentiation**  
381 **of neural crest cells into vascular smooth muscle cells.**

382 In the *Tbx1*<sup>+/-</sup> mouse model of 22q11 deletion syndrome, PAA formation recovers in 50  
383 – 68% of the mutant mice<sup>49, 50</sup>. To determine whether the rearrangement of the  
384 endothelial plexus in the 4<sup>th</sup> arch was blocked or delayed, we examined E11.5 embryos.  
385 The incidence of IAA-B and RERSA in integrin  $\alpha 5$ <sup>f/-</sup>; *Isl1*<sup>Cre</sup> mutants is 50%, which is the  
386 same as the incidence of defective 4<sup>th</sup> PAA formation. Therefore, we expected to find  
387 absent or thin 4<sup>th</sup> PAAs in the mutants at E11.5. Contrary to our expectations, the  
388 formation of the 4<sup>th</sup> PAAs recovered in the mutants by E11.5, and PAA perimeters in the  
389 mutants were comparable with controls (Fig. 7A, n=8). Consistent with the recovery of  
390 SHF-derived ECs numbers by 33 – 35s, PAA ECs were GFP<sup>+</sup> cells in the mutants as in  
391 controls (compare Fig. 7C1 with 7D1, arrowheads). Regression of left 4<sup>th</sup> PAAs results  
392 in IAA-B and regression of the right 4<sup>th</sup> results in RERSA<sup>51, 52</sup>. Since 50% of *integrin*  
393  *$\alpha 5$* <sup>flox/-</sup>; *Isl1*<sup>Cre</sup> mutants develop 4<sup>th</sup> arch artery defects, such as IAA-B and RERSA<sup>29</sup>,  
394 these data indicated that the 4<sup>th</sup> PAAs eventually regress in the mutants. Arch artery  
395 regression is commonly caused by the defective differentiation of neural crest cells

396 surrounding the PAA endothelium into vascular smooth muscle cells, VSMCs<sup>52-57</sup>. In  
397 pharyngeal arches, VSMCs exclusively arise from NC-derived cells<sup>49, 58, 59</sup>. To  
398 determine whether the differentiation of NC-derived cells into VSMCs was affected in  
399 our mutants, we analyzed VSMC differentiation in the pharyngeal arches. For these  
400 experiments, we calculated the fraction of vessel perimeter covered by alpha smooth  
401 muscle actin ( $\alpha$ SMA)-expressing cells, using previously-developed methodology<sup>31</sup>. We  
402 found that the differentiation of NC-derived cells into VSMCs was severely diminished  
403 around the PAAs in the mutants (quantified in Fig. 7B; compare sections in Fig. 7C, D,  
404 magnified in Fig. 7C2, D2; zoom-out panels are in Sup. Fig. 6). The decrease in  $\alpha$ SMA  
405 expression was not due to NC cell death (Sup. Fig. 2).

406 Even though, the *Isl1* lineage marks a subset NC-derived cells<sup>60</sup>, Isl1 protein is not  
407 expressed in NC-lineage cells in the pharyngeal arches, and Isl1 lineage does not label  
408 cells adjacent to the PAA endothelium (Fig. 7C1, D1)<sup>29</sup>. Moreover, comparison of NC  
409 lineage (Fig. 7E – E4) and Isl1 lineage maps at E11.5 demonstrates that  $\alpha$ SMA  
410 expression coincides with the NC lineage (Fig. 7E2), but not with Isl1 lineage-labeled  
411 cells (arrows in Fig. 7C1 and C2 point to  $\alpha$ SMA-expressing cells; arrowheads point to  
412 GFP<sup>+</sup> PAA endothelium). These studies indicate that the expression of integrin  $\alpha$ 5 in the  
413 Isl1 lineage(s) regulates the differentiation of NC cells into VSMCs in a non-cell  
414 autonomous manner. These results are consistent with our previous experiments  
415 demonstrating that the expression of integrin  $\alpha$ 5 in the *Mesp1* lineage marking the  
416 anterior mesoderm regulates the differentiation of NC cells into VSMCs around the 4<sup>th</sup>  
417 PAA<sup>59</sup>. Since the deletion of integrin  $\alpha$ 5 in the *Mesp1* lineage does not result in  
418 defective or delayed PAA formation<sup>59</sup>, these data taken together, indicate that the

419 defect in VSMC differentiation in *integrin  $\alpha 5^{flox/-}; Isl1^{Cre}$*  mutants is not merely due to the  
420 delayed accrual of arch artery endothelium, or delayed remodeling of the vascular  
421 plexus into the PAA. In summary, our studies also indicate that in addition to regulating  
422 4<sup>th</sup> PAA formation, integrin  $\alpha 5$  expressed in the *Isl1* lineages plays an independent role  
423 in arch artery morphogenesis, namely in the differentiation of NC-derived cells into  
424 VSMCs (Fig. 8A).

425 The differentiation of NC into VSMCs is orchestrated in part by a relay of Notch  
426 signaling transduced from the PAA endothelium to the surrounding layers of NC-derived  
427 cells<sup>56</sup>. The activation of Notch signaling in the NC is required for the differentiation of  
428 NCs into VSMCs<sup>52, 56</sup>. We demonstrated that this pathway was regulated by the  
429 expression of integrin  $\alpha 5$  and fibronectin specifically by NC-derived cells at E11.5<sup>31</sup>. To  
430 test the possibility that the expression of integrin  $\alpha 5$  in the *Isl1* lineages regulates the  
431 lateral propagation of Notch from the PAA endothelium to the adjacent NC-derived cells,  
432 we stained control and mutant sections with an antibody to Notch Intracellular Domain  
433 (NICD), an activated form of Notch. However, Notch signaling was activated  
434 comparably in controls and mutants, despite the severe deficiency in the differentiation  
435 of NC cells into VSMCs in the mutants (compare Fig. 7C2 – C4 with Fig. 7D2 – D4,  
436 arrows). These experiments indicate that the expression of integrin  $\alpha 5$  in the pharyngeal  
437 arch mesoderm regulates the differentiation of NC cells into VSMCs independently of  
438 Notch. Furthermore, these experiments indicate that while the activation of Notch is  
439 necessary for the differentiation of NC-derived cells into VSMCs, it is not sufficient.  
440 Taken together, with our previous work<sup>31, 59</sup>, studies in this manuscript demonstrate that

441 cell-ECM interactions regulated by integrin  $\alpha5\beta1$  and Fn1 play multiple, pleiotropic, and  
442 stage-specific functions during the morphogenesis of the 4<sup>th</sup> PAAs (Fig. 8).

443 **Combinatorial expression of integrin  $\alpha5$  and fibronectin from multiple lineages in**  
444 **the pharynx regulates the formation of the 4<sup>th</sup> PAAs.**

445 The *Isl1* lineages encompass the mesoderm in the SHF and pharyngeal arches,  
446 pharyngeal endoderm, surface ectoderm, and some NC-derived cell populations,  
447 although not the NC in the pharyngeal arches<sup>29, 42, 59, 60</sup>. Our previous studies indicated  
448 that the combined expression of integrin  $\alpha5\beta1$  or Fn1 in the surface ectoderm and the  
449 NC was not required for the formation of the 4<sup>th</sup> PAAs<sup>29, 31</sup>. However, even though PAA  
450 formation occurred normally in these mice, the 4<sup>th</sup> PAAs regressed later due to defects  
451 in the differentiation of NC-derived cells into VSMCs, resulting in RERSA and IAA-B<sup>31</sup>  
452 (Fig. 8). The expression of either integrin  $\alpha5\beta1$  or Fn1 in the SHF lineage marked by the  
453 expression of the *Mef2C-AHF-Cre* transgene is also not required for PAA formation  
454 (Sup. Tables 1 and 2), indicating that the expression of integrin  $\alpha5\beta1$  or Fn1 in the SHF  
455 alone is not required for cardiovascular development. Consistent with these findings, the  
456 expression of integrin  $\alpha5\beta1$  in the *Mesp1* lineage or in the endothelium was not required  
457 for PAA formation<sup>59, 61</sup> (Fig. 8). Instead, the expression of integrin  $\alpha5\beta1$  in the *Mesp1*  
458 lineage was required for PAA stability, and the deletion of integrin  $\alpha5$  in *Mesp1* lineage  
459 which includes the PAA endothelium resulted in IAA-B and RERSA (Fig. 8)<sup>59, 61</sup>.

460 The difference in the phenotypes resulting from the deletion of integrin  $\alpha5$  using *Mef2C-*  
461 *AHF-Cre* and *Mesp1*<sup>Cre</sup> are likely the result of differences in the timing of Cre expression  
462 (e.g. the later onset of *Mef2C-AHF-Cre* may have allowed the perdurance of integrin

463  $\alpha 5\beta 1$  protein through the stages where it's required for mesoderm-NC interactions).  
464 Alternatively, the expression of integrin  $\alpha 5\beta 1$  in *Mesp1* lineage-derived mesodermal  
465 cells prior to E8.5 is important for the regulation of NC cell fate in the pharyngeal arches  
466 <sup>59</sup>.

467 Lastly, we tested whether the expression of integrin  $\alpha 5$  in the endoderm regulated PAA  
468 formation. For these experiments, we used the constitutive *Sox17*<sup>2A-iCre</sup> knockin mouse  
469 line, in which Cre is expressed in the endoderm and pharyngeal arch ECs (Sup. Fig. 7A  
470 – A4) <sup>62</sup>. However, PAAs formed normally in  *$\alpha 5^{fllox/-}; Sox17^{2A-iCre}$*  mutants (Sup. Fig. 7B,  
471 B1, C, C1). Together, these data indicate that combinatorial expression of integrin  $\alpha 5$   
472 and *Fn1* in the *Isl1* lineages is necessary for the proper formation of the 4<sup>th</sup> PAAs (Fig.  
473 8).

474

## 475 Discussion

476 Proper development of the 4<sup>th</sup> PAAs is central to the ability of a newborn to survive and  
477 thrive (Karunamuni et al., 2014; Moon, 2008). The formation of the 4<sup>th</sup> pair of the PAAs  
478 is regulated by a number of genes including *Tbx1*, *Pax9*, *Gbx2*, *Fgf8*, *Crkl*, *PlexinD1*,  
479 and *Nrp1*, e.g., <sup>63-67</sup>. However, cellular mechanisms by which these genes mediate PAA  
480 formation are not well-understood. Unraveling the dynamics of EC progenitors and their  
481 descendants during PAAs formation is vital to understanding the genetic and cellular  
482 mechanisms regulating PAA formation and how they are altered in congenital heart  
483 disease.

484 In this manuscript, we have demonstrated that the SHF is the primary source of the  
485 PAA endothelium and that the majority of endothelial progenitors giving rise to the PAAs  
486 are already present in the SHF by E7.5. PAA progenitors exit the SHF and contribute to  
487 the PAAs over a span of about 2 days, from E7.5 to E9.5.

488

489 Lineage labeling using constitutive Cre lines *Isl1<sup>Cre</sup>* and *Mef2C-AHF-Cre* led to similar  
490 labeling of the PAA endothelium, with the exception of the 3<sup>rd</sup> PAA, which is labeled  
491 50% more efficiently when *Isl1<sup>Cre</sup>* line of mice is used. This difference likely reflects the  
492 timing of Cre expression in *Isl1<sup>Cre</sup>* and *Mef2C-AHF-Cre* strains, with *Mef2C-AHF-Cre*  
493 lagging by about a day<sup>42, 48, 68</sup>. The difference in the labeling efficiency suggests that  
494 about half of the endothelial progenitors of the 3<sup>rd</sup> PAAs have exited the SHF by the  
495 time *Mef2C-AHF-Cre* is expressed. Our fate mapping studies show that there are  
496 differences in the timing and the extent of SHF contribution to the PAAs. In particular, if  
497 one were to use *Mef2C-AHF-Cre* to generate mutations, the 4<sup>th</sup> PAAs could be more  
498 affected than the 3<sup>rd</sup> and the 6<sup>th</sup> because in the *Mef2C-AHF-Cre* strain, the contribution  
499 of the SHF lineage-labeled ECs to the 4<sup>th</sup> PAA endothelium is the highest.

500 By using whole-mount imaging and quantitative analyses of EC populations in the  
501 pharyngeal arches, we previously demonstrated that the morphogenesis of the 4<sup>th</sup> PAAs  
502 occurs gradually throughout the 10<sup>th</sup> day of the embryonic development and entails a  
503 rapid accumulation of ECs: endothelial population in the 4<sup>th</sup> pharyngeal arch increases  
504 more than three-fold in about eight hours of development, from 30 – 39 somites<sup>9</sup>. This

505 steep increase is unlikely to occur solely due to EC proliferation, and our labeling  
506 experiments show that SHF-derived cells are still being added to the 4<sup>th</sup> PAA after E9.5.  
507 Our studies show that integrin  $\alpha 5\beta 1$  and Fn1 are important for initial recruitment of SHF-  
508 derived ECs into the 4<sup>th</sup> pharyngeal arches, and that in the absence of integrin  $\alpha 5$  or  
509 Fn1 in the *Isl1* lineages results in EC deficiency up to 32 – 34 somite stage. Despite the  
510 initial EC deficiency in the 4<sup>th</sup> arch, EC numbers recover in integrin  $\alpha 5^{f/-}$ ; *Isl1*<sup>Cre/+</sup> and  
511 *Fn1*<sup>f/-</sup>; *Isl1*<sup>Cre/+</sup> mutants by the 34 – 35 somite stage. We demonstrate that the recovery  
512 of EC cell numbers in the pharyngeal arches is not due to compensation from an  
513 alternative endothelial source. Instead, we show that the proliferation index of plexus  
514 endothelium is 2-fold higher than that of ECs in the 4<sup>th</sup> PAA (Fig. 3O). This difference in  
515 the proliferation index is maintained in the mutants (Fig. 3O). We hypothesize that since  
516 the majority of ECs is in the plexus at 32 – 33 somites in the mutants, their proliferative  
517 advantage over ECs in the PAA allows the EC number in the mutant arches to recover  
518 by the end of E10.5.

519 In spite of the recovery of EC populations in the 4<sup>th</sup> arches, the 4<sup>th</sup> PAAs were either thin  
520 or absent in 50% of all the 4<sup>th</sup> arches by 36 – 39 somite stages<sup>29</sup>. Our regression  
521 analysis showed that the rearrangement of the 4<sup>th</sup> pharyngeal arch ECs into the PAA  
522 was not dependent on the number or density of ECs in the 4<sup>th</sup> arch. These data suggest  
523 that the remodeling of the uniform endothelial plexus into the PAA in the 4<sup>th</sup> arch is  
524 mediated by factors extrinsic to the endothelium. The disruption of the remodeling in our  
525 mutants indicates an essential role for cell – ECM interactions in this process.

526



527 The *Isl1* lineage encompasses multiple cell types within the pharynx including  
528 pharyngeal epithelia, mesoderm, and a population of NC cells in the cardiac outflow  
529 tract<sup>60, 68</sup>. Pharyngeal endoderm and the ectoderm are important signaling centers  
530 regulating intercellular communications among the germ layers composing the arches  
531 during the morphogenesis of cardiopharyngeal organs and structures<sup>27, 69, 70</sup>.  
532 Modulation of the extracellular microenvironment within the pharynx is essential for the  
533 development cardiovascular system<sup>29, 31, 59, 63, 64, 71-81</sup>. The expression of *Fn1*, an  
534 essential ECM glycoprotein, is highly enriched in the pharyngeal epithelia<sup>28, 29</sup>, and our  
535 studies show that signaling by Fn1 in the *Isl1* lineages is important for the accrual of  
536 SHF-derived cells to the pharyngeal mesenchyme, and for the formation of the 4<sup>th</sup>  
537 PAAs. In the latter step, signaling by Fn1 in tissues extrinsic to the pharyngeal arch  
538 endothelium regulates the remodeling of endothelial plexus into the PAA in the 4<sup>th</sup> arch.  
539 While Fn1 expression in the NC regulates PAA stability after the 4<sup>th</sup> PAA has formed<sup>29</sup>,  
540<sup>31</sup> (Fig. 8).

541

542 In this manuscript, we investigated the tissues wherein signaling by Fn1 is important for  
543 PAA formation. Integrin  $\alpha5\beta1$  is a major Fn1 receptor during embryogenesis<sup>28-30, 34, 38</sup>,  
544<sup>39, 41</sup>, and the deletion of integrin  $\alpha5$  or Fn1 in the *Isl1* lineages results in identical  
545 phenotypes<sup>29</sup>. To determine the cell type(s) in which signaling by Fn1 regulates PAA  
546 formation, we ablated integrin  $\alpha5$  in each of the tissues comprising *Isl1* lineage  
547 individually or in combination. The deletion of integrin  $\alpha5$  in the SHF (*Mef2C-AHF-Cre*  
548 strain), the entire anterior mesoderm (*Mesp1<sup>Cre</sup>*), the NC (*Wnt1-Cre2*, *P3Pro-Cre*), the

549 NC and surface ectoderm (TFAP2 $\alpha$ <sup>lresCre</sup>), or the endoderm and endothelia (Sox17<sup>2A-</sup>  
550 <sup>iCre</sup>) resulted in normal PAA formation (this study and <sup>29, 31, 59</sup>). Therefore, we conclude  
551 that combinatorial signaling by integrin  $\alpha$ 5 $\beta$ 1 from pharyngeal endoderm, mesoderm,  
552 and the surface ectoderm is essential to mediate the formation of the 4<sup>th</sup> PAAs. While  
553 signaling in the mesoderm and the neural crest is important for PAA stability (Fig. 8).

554

555 The PAAs form within the neural crest-derived pharyngeal mesenchyme and the PAA  
556 endothelium induces the differentiation of the adjacent NC-derived cells into VSMCs <sup>56</sup>.  
557 Despite the initial delay in the formation of the 4<sup>th</sup> PAAs, the size of PAAs in integrin  $\alpha$ 5<sup>f/-</sup>  
558 ; Isl1<sup>Cre/+</sup> mutants recovers by E11.5. At this time, we observed a profound deficiency in  
559 the expression of  $\alpha$ SMA by NC-derived cells around the PAAs in the mutants.  
560 Deficiency in VSMC differentiation causes vessel regression <sup>31, 52, 57, 82, 83</sup>, consistent  
561 with our finding that integrin  $\alpha$ 5<sup>f/-</sup>; Isl1<sup>Cre/+</sup> and Fn1<sup>f/-</sup>; Isl1<sup>Cre/+</sup> mutants develop IAA-B and  
562 RERSA; defects that are caused by the aberrant morphogenesis of the left and right 4<sup>th</sup>  
563 PAAs, respectively <sup>29</sup>. Our previous studies using integrin  $\alpha$ 5<sup>f/-</sup>; Mesp1<sup>Cre/+</sup> mice  
564 demonstrated that the expression of integrin  $\alpha$ 5 in the mesoderm regulates NC  
565 differentiation into VSMCs without affecting PAA formation, and integrin  $\alpha$ 5<sup>f/-</sup>; Mesp1<sup>Cre/+</sup>  
566 mice develop IAA-B and RERSA <sup>59</sup> (Fig. 8). Thus, the roles of integrin  $\alpha$ 5 $\beta$ 1 and Fn1 in  
567 the formation of the 4<sup>th</sup> PAAs are separate from their roles in the differentiation of NC-  
568 derived cells into VSCMs <sup>31</sup>.

569

570 Mechanisms that lead to IAA-B are complex but generally arise due to either of the  
571 following two broad categories of defects: a) defects in the formation of the left 4<sup>th</sup> PAA  
572 or b) defects in the stability of an otherwise well-formed 4<sup>th</sup> PAA. NC ablation studies in  
573 chick and genetic manipulation of the neural crest demonstrate that NC is not required  
574 for PAA formation<sup>51, 52</sup>. Even in the extreme case of neural crest ablation, PAAs form<sup>51</sup>.  
575 However, defective differentiation of NC-derived cells into VSMCs leads to PAA  
576 regression resulting in various malformations in the aortic arch and its branches,  
577 including IAA-B and RERSA<sup>31, 52, 82</sup>. Our studies show that the expression of integrin  
578  $\alpha 5\beta 1$  in the pharyngeal mesoderm and the NC are required for NC-to-VSMC  
579 differentiation, and the expression of integrin  $\alpha 5\beta 1$  in either of these lineages alone is  
580 not sufficient for this process<sup>31, 59</sup>.

581  
582 Defects in the formation of the 4<sup>th</sup> PAAs often occur in conjunction with 22q11 deletion  
583 syndromes<sup>84</sup>. Cumulatively, four prospective studies found that between 40 and 90% of  
584 interrupted aortic arch type B (IAA-B) cases diagnosed in fetuses, neonates, and  
585 children can be attributed to deletions in the 22q11 region<sup>85</sup>. Studies using *Tbx1*<sup>+/-</sup> mice  
586 that model 22q11 deletion syndrome indicated that defective formation of the left 4<sup>th</sup>  
587 PAA underlies IAA-B in these patients<sup>65, 86, 87</sup>. Intriguingly, several independent  
588 publications demonstrated that *Tbx1* regulates the expression of integrins and  
589 extracellular matrix (ECM) components, and showed that defects in cell-ECM  
590 interactions downstream of *Tbx1* precede pathological sequelae and cardiovascular  
591 defects in *Tbx1* mutants<sup>71-73</sup>. Interestingly, about 50% of *Tbx1*<sup>+/-</sup> mice recover from the  
592 initial defect in PAA formation, and are viable and fertile<sup>50</sup>; However, this recovery can

593 be impeded by the reduction in the expression of Fn1<sup>49</sup>. Thus, alterations in cell-ECM  
594 interactions and pharyngeal ECM microenvironment may underlie lethal AAA defects in  
595 22q11 deletion syndrome downstream of *Tbx1*.

596 The significance of our work lies in the identification of cellular dynamics regulating PAA  
597 formation and the intricate temporal and cell-type specific roles of cell-ECM interactions  
598 in the regulation of aortic arch morphogenesis at multiple steps of its formation and  
599 remodeling (Fig. 8).

600

601 **Acknowledgements** We thank Richard Hynes, Chenleng Cai, Sylvia Evans, Benoit  
602 Bruneau, Heicko Lickert, and Hongkui Zeng for the gift of mouse strains, and Brianna  
603 Alexander and Nathan Astrof for careful reading of the manuscript.

604

605 **Sources of Funding** This work was supported by the funding from the National Heart,  
606 Lung, and Blood Institute of the NIH R01 HL103920, R01 HL134935, and R21  
607 OD025323-01 to SA, and pre-doctoral fellowship F31HL150949 to AJR.

608 **Disclosures** None

609 **Supplemental Materials**  
610 Expanded Materials & Methods  
611 Online Figures 1 – 7

612 **Figure Legends**

613 *Figure legends are also included with the figures*

614 **Figure1. Endothelial PAA progenitors are arise in the SHF as early as E7.25.**

615 *Isl1*<sup>MerCreMer</sup> and *Mef2C-AHF-DreERT2* males were mated with the appropriate reporter  
616 females (see Methods). E0.5 was considered to be noon on the day of the vaginal plug.  
617 Tamoxifen was injected at specified times, embryos were dissected at E10.5, and  
618 stained to detect VEGFR2 (blue), ERG (red), or tdTomato (orange). **A.** Sagittal view and  
619 3D reconstruction through the left pharyngeal region. Inset- 3D reconstruction of PAAs.  
620 **A1 – A2.** Sagittal optical sections through the embryo shown in **A.** Labeling efficiency  
621 was quantified by calculating the ratio of the number of ERG<sup>+</sup> tdTomato<sup>+</sup> ECs to the  
622 total number of ERG<sup>+</sup> ECs in PAAs using IMARIS spot function. **B.** Highest labeling of  
623 PAA endothelium occurred when tamoxifen was injected at E7.25 in *Isl1*<sup>MerCreMer</sup> knockin  
624 mice. **B1.** SHF-derived cells continue to be added the 4<sup>th</sup> PAA after E9.5. **C.** Peak  
625 labeling of PAA ECs occurred when tamoxifen was injected at E8.0 in *Mef2C-AHF-*  
626 *DreERT2* strain. **C1.** Injection of tamoxifen at E8.5 led to a more efficient labeling of the  
627 4<sup>th</sup> PAAs than the 3<sup>rd</sup> and 6<sup>th</sup> PAAs.

628 **Figure 2. Majority of PAA ECs are SHF-derived; there are differences in the**  
629 **contribution of the SHF to the PAA endothelium depending on the strain used.**

630 *Mef2C-AHF-Cre*; *ROSA*<sup>tdTomato</sup> embryos (35 – 37 somites) were stained with antibodies  
631 to VEGFR2 (turquoise) to detect endothelial cells, tdTomato (orange) to detect SHF-  
632 derived cells, and DAPI (blue) to stain cell nuclei. **A – A2.** 3D reconstructions of PAAs  
633 and their connections with the dorsal aorta (dAo) and the aortic sac (Ao S). **B – B2.**

634 Sagittal optical sections to show the distribution of all SHF-derived cells in the  
635 pharyngeal arches. PAAs 3 – 6 are labeled. Magnifications are the same in all panels.  
636 All scale bars are 100  $\mu\text{m}$ . **C.** The number of VEGFR2<sup>+</sup>EGR<sup>+</sup> cells in the pharyngeal  
637 arches was quantified in 5 E10.5 embryos at 35 – 37 somites using IMARIS. Each dot is  
638 one arch. Red line marks the median. Black lines mark quartiles. Differences among the  
639 three PAA pairs are not significant,  $p > 0.1$  by one-way ANOVA with Tukey's correction  
640 for multiple testing. **D – E.** The percentage of VEGFR2<sup>+</sup>EGR<sup>+</sup> cells expressing the Cre  
641 reporter was determined in each PAA (orange bars). Blue bars are the percent of  
642 VEGFR2<sup>+</sup>EGR<sup>+</sup> cells that were not labeled with the Cre reporter. **D.** The use of  
643 constitutive *Isl1*<sup>Cre</sup> strain resulted in labeling of more than 80% of ECs in the 3<sup>rd</sup> and 4<sup>th</sup>  
644 PAAs. **E.** The use of *Mef2C-AHF-Cre* strain resulted in a significantly higher labeling of  
645 the 4<sup>th</sup> PAAs than the 3<sup>rd</sup> and the 6<sup>th</sup>. The difference in the labeling efficiency of 6<sup>th</sup>  
646 PAAs between the two strains was not significant,  $p > 0.2$ . All statistical analyses were  
647 performed using one-way ANOVA with Tukey's correction for multiple testing.

648

649 **Figure 3. Formation of the 4<sup>th</sup> PAA is delayed in integrin  $\alpha 5^{\text{flox}/-}$ ; *Isl1*<sup>Cre</sup> mutants.**

650 Integrin  $\alpha 5^{\text{flox}/+}$ ; *Isl1*<sup>Cre</sup> control and  $\alpha 5^{\text{flox}/-}$ ; *Isl1*<sup>Cre</sup> mutant embryos were dissected at  
651 different somite stages at E10.5 and stained to detect *Pecam1*. PAAs are numbered  
652 and somite stages are indicated in the first row. **A, D, G, J.** 3D reconstructions of whole-  
653 mount *Pecam 1* staining (light blue). **B, E, H, K.** PAA endothelium in the 3<sup>rd</sup>, 4<sup>th</sup> and 6<sup>th</sup>  
654 arches shown in the row above was surface-rendered white, green and red,  
655 respectively. In addition, the plexus endothelium in the 4<sup>th</sup> arch was surface-rendered in  
656 pink. **C, F, I, L.** Left side and ventral views of surface-rendered PAAs and the plexus.

657 Development of the 4<sup>th</sup> PAAs was specifically affected in the mutants (**E, F**).  
658 Magnification is the same in all panels. Scale bar is 100  $\mu$ m. **M**. Total number of  
659 endothelial cells was quantified as described in Methods. Mutants have EC deficiency in  
660 the 4<sup>th</sup> arch as 32 – 33 somites. **N**. The sizes of the 4<sup>th</sup> arches are comparable between  
661 controls and mutants. **O**. EC proliferation in the PAA and the plexus in the 4<sup>th</sup> arches  
662 was similar in controls (C) and mutants (M). In all plots, solid lines mark the median,  
663 dashed lines mark the quartiles. Each dot marks one arch. At least 3 mutants and 3  
664 controls were assayed. Statistics were evaluated using 2-tailed, unpaired Student's t  
665 test with Welch's correction for unequal standard deviation between samples.

666

667 **Figure 4. The expression of integrin  $\alpha 5$  in the *Isl1* lineages is required for the**  
668 **accrual of SHF-derived cells to the pharyngeal mesenchyme.** Control and mutant  
669 embryos carrying one ROSA<sup>nTnG</sup> reporter allele were dissected at E9.5 (18 – 20 somite  
670 stage) and stained with DAPI and anti-GFP antibodies. Whole embryos were imaged  
671 and the number of GFP<sup>+</sup> cells (SHF-derivatives) in the arch mesenchyme, splanchnic  
672 mesoderm, and in the heart was quantified as described in Sup. Fig. 4. **A**. The total  
673 number of SHF cells in the mesenchyme of the 1<sup>st</sup> and 2<sup>nd</sup> arches was decreased in the  
674 mutants. **B**. The total number of of GFP<sup>+</sup> cells in the pharyngeal mesenchyme  
675 corresponding with the future arches 3 – 6 was decreased in the mutants. The number  
676 of SHF cells in heart (**C**) and the splanchnic mesoderm (**D**) was not affected. **E**. The  
677 proportion of GFP<sup>+</sup> cells in the heart relative to GFP<sup>+</sup> cells in splanchnic mesoderm was  
678 not affected in the mutants. **F**. The proportion of GFP<sup>+</sup> cells in the posterior pharyngeal  
679 mesenchyme relative to the number of GFP<sup>+</sup> cells in splanchnic mesoderm was

680 significantly decreased in the mutants. Each dot marks one embryo, red lines mark  
681 medians, dotted lines mark quartiles; p values were determined using unpaired, 2-tailed  
682 Student's t tests.

683

684 **Figure 5. Recovery of EC numbers in integrin  $\alpha 5^{\text{flox/-}}$ ;  $\text{Isl1}^{\text{Cre/+}}$  mutants. A.** Total EC  
685 number has recovered in integrin  $\alpha 5^{\text{flox/-}}$ ;  $\text{Isl1}^{\text{Cre/+}}$  mutants by the 34<sup>th</sup> somite stage. **B.**  
686 Total number of SHF-derived mesodermal cells has recovered in the pharyngeal arches  
687 in integrin  $\alpha 5^{\text{flox/-}}$ ;  $\text{Isl1}^{\text{Cre/+}}$  mutants by the 34<sup>th</sup> somite stage. **C.** The fraction of SHF-  
688 derived ECs in pharyngeal arches is comparable among control and mutant embryos.  
689 This fraction was calculated by quantifying the number of GFP<sup>+</sup>ERG<sup>+</sup> cells and dividing  
690 by the total number of ERG<sup>+</sup> cells in the entire pharyngeal arches (e.g. ECs in PAA and  
691 plexus were quantified). Statistical significance was evaluated using one-way ANOVA  
692 with Tukey's correction for multiple testing.

693

694 **Figure 6. Integrin  $\alpha 5\text{b1}$  and  $\text{Fn1}$  regulate the remodeling of EC plexus during the**  
695 **formation of the 4<sup>th</sup> pharyngeal arch arteries. A.** The proportion of ECs in the 4<sup>th</sup>  
696 PAAs in the mutant is significantly lower than in controls at all stages analyzed at E10.5,  
697 including the stages when the EC population in the 4<sup>th</sup> pharyngeal arch has recovered in  
698 the mutants; 2-tailed, unpaired Student's t test. **B – C.** Linear regression analyses  
699 indicate the absence of linear correlation between the size of the 4<sup>th</sup> PAA and EC  
700 number (**B**) or density (**C**). PAA size is expressed as the percentage of pharyngeal arch  
701 endothelial cells in the 4<sup>th</sup> PAA in control embryos on the y-axis. **D.** Total EC number (x-



702 axis) from mutants with defective (open symbols) or unaffected 4<sup>th</sup> PAA (closed  
703 symbols) were plotted against the size of the 4<sup>th</sup> PAAs, y -axis. Regression analysis  
704 indicated low correlation between these properties. Circles: 32 – 33 somite embryos,  
705 rhombi: 34 – 35 somite embryos, triangles: 36 – 39 somite embryos. **E.** The  
706 rearrangement of the endothelial plexus into the 4<sup>th</sup> PAAs is defective in mutants  
707 relative to controls with the same number of endothelial cells in the 4<sup>th</sup> arch (red boxes).  
708 EC – endothelial cell(s). Controls:  $\alpha 5^{fl/+}$ ;  $Isl1^{Cre/+}$  and  $Fn1^{fl/+}$ ;  $Isl1^{Cre/+}$  embryos; Mutants:  
709  $\alpha 5^{fl/-}$ ;  $Isl1^{Cre/+}$  and  $Fn1^{fl/-}$ ;  $Isl1^{Cre/+}$  embryos.

710 **Figure 7. The expression of integrin  $\alpha 5\beta 1$  in the  $Isl1$  lineages regulates the**  
711 **differentiation of neural crest-derived cells into VSCMs at E11.5** **A.** PAA perimeter  
712 has recovered in size in the mutants by E11.5. **B.** Smooth muscle coverage of the left  
713 4<sup>th</sup> and left 6<sup>th</sup> PAA was deficient in the mutants. **C – D.** Despite defective differentiation  
714 of NC cells into VSMCs, the activation of Notch in the pharyngeal arch mesenchyme  
715 was not altered in the mutants. PAAs are numbered. PAA lumens at E11.5 are derived  
716 from the  $Isl1^{Cre}$  lineage (green, arrowheads in **C1** and **D1**).  $\alpha$ SMA<sup>+</sup> cells are GFP-  
717 negative in  $Isl1^{Cre}$  strain (arrows in **C1-C2**). **C2 – D2.** VSMC differentiation assayed by  
718 the expression of alpha smooth muscle actin ( $\alpha$ SMA, blue) is specifically affected  
719 around the 4<sup>th</sup> PAAs in the mutants (compare regions marked by the arrows in **C2** and  
720 **D2**). The activation of Notch assayed by the expression of NICD is not altered in the  
721 mutants with defective VSCM differentiation (arrows in **C3, C4** and **D3, D4**). **E.** Fate  
722 map using  $TFAP2\alpha^{IRESCre}$  shows the location of NC-derived cells in the pharyngeal  
723 arches. Note extensive colonization of the mesenchyme between the endodermal  
724 pouches (endo) by the  $TFAP2\alpha^{IRESCre}$  lineage. **E2.**  $\alpha$ SMA<sup>+</sup> cells are GFP<sup>+</sup> in

725 TFAP2 $\alpha$ <sup>IRES<sup>Cre</sup></sup> strain. All scale bars are 50  $\mu$ m. Additional zoom-out views are in Sup.  
726 Fig. 6.

727

728 **Figure 8. Cell – ECM interactions play essential roles at multiple stages during the**

729 **development of the aortic arch and its branches. A.** The expression of integrin  $\alpha$ 5 $\beta$ 1

730 and Fn1 in the Isl1 lineages is required for the formation of the 4<sup>th</sup> PAAs. **A1.** A

731 schematic of Isl1 lineages (green) in the pharynx at E8.5 – E9.5. Green arrows indicate

732 migration of splanchnic mesoderm cells into the pharyngeal arches. Red lines signify

733 enriched localization of Fn1 protein at germ layer borders. Integrin  $\alpha$ 5 $\beta$ 1 is expressed in

734 all cell types in the pharynx at E8.5 (Chen et al., 2015) and regulates the accrual of

735 pharyngeal mesoderm from the SHF (green arrows). **A2.** During the 10<sup>th</sup> day of mouse

736 development, integrin  $\alpha$ 5 $\beta$ 1 and Fn1 regulate the remodeling of the plexus endothelium

737 in the 4<sup>th</sup> pharyngeal arch into the PAA. Isl1 lineages are marked in green. NC-derived

738 cells are in blue. **B.** The expression of integrin  $\alpha$ 5 in the mesoderm regulates the

739 differentiation of NC-derived cells into VSMCs. The deletion of integrin  $\alpha$ 5 in Mesp1

740 lineage, which includes the SHF, leads to defective NC-to-VSMC differentiation and

741 results in the regression of the 4<sup>th</sup> PAAs leading to IAA-B and RERSA (Liang, et al., *Dev*

742 *Biol* 2014). **C.** Fn1 becomes upregulated in NC-derived cells adjacent to the 4<sup>th</sup> PAA

743 ECs between E10.5 and E11.5 The expression of integrin  $\alpha$ 5 $\beta$ 1 and Fn1 in the NC-

744 derived cells is required for NC-to-VSMC differentiation and the stability of the 4<sup>th</sup> PAA

745 (Wang et al, 2016). The deletion of either  $\alpha$ 5 or Fn1 in the NC (and the surface

746 ectoderm) leads to IAA-B and RERSA but does not impair PAA formation.

747

748 **Supplemental Figure 1. Delayed formation of the 4<sup>th</sup> PAAs in mutants lacking**  
749 **integrin  $\alpha 5$  or Fn1 in the Isl1 lineages. A – B.** Quantification of total endothelial cell  
750 numbers in the 4<sup>th</sup> arches of controls and mutants show similar phenotypes among  
751 integrin  $\alpha 5^{\text{flox/-}}$ ; Isl1<sup>Cre/+</sup> and Fn1<sup>flox/-</sup>; Isl1<sup>Cre/+</sup> embryos. Note the recovery of endothelial  
752 cell numbers at 36 – 40-somite stage. **C.** Combined data comparing endothelial  
753 populations of controls and integrin  $\alpha 5^{\text{flox/-}}$ ; Isl1<sup>Cre/+</sup> and Fn1<sup>flox/-</sup>; Isl1<sup>Cre/+</sup> mutant embryos  
754 at 33 – 34-somite stages. **D.** The proportion of pharyngeal ECs in the plexus is  
755 increased in the mutants relative to controls. **E.** The proportion of endothelial cells in the  
756 PAA is decreased in the mutants relative to controls. Note, 7 of 16 mutants did not have  
757 PAAs (0% endothelial cells in the 4<sup>th</sup> PAA).

758

759 **Supplemental Figure 2. The prevalence of cell death, as assayed by the presence**  
760 **of cleaved caspase 3 or TUNEL signals, was similar in controls and mutants. A, C.**  
761 Controls. **B, D.** Mutants. All scale bars are 100  $\mu\text{m}$ .

762

763 **Supplemental Figure 3. The differentiation of SHF-derived cells into endothelial**  
764 **cells is not affected by the deletion of integrin  $\alpha 5$  in the Isl1 lineages.** Whole-mount  
765 staining, confocal imaging and 3D reconstruction through the pharyngeal regions of  
766 control (**A, C**) and mutant (**B, D**) embryos. **A – B.** Sagittal optical sections through E9.5  
767 embryos: The majority of VEGFR2<sup>+</sup> cells express GFP and ERG in the 3<sup>rd</sup> PAA and in a  
768 more posterior mesenchyme (arrows) in controls and mutants. **C – D.** E10.5 embryos.  
769 3D reconstruction through the pharyngeal region. Open chevrons mark the 4<sup>th</sup> PAAs.

770 Note the presence of a very thin PAA in the mutant (**D-D1**). All VERGFR2<sup>+</sup> cells are  
771 Pecam1<sup>+</sup> in control and in the mutant with defective 4th PAA. Scale bars are 50 μm.

772

773 **Supplemental Figure 4. Quantification of SHF-derived cells in pharyngeal**

774 **mesenchyme and splanchnic mesoderm.** E9.5 *Isl1<sup>Cre/+</sup>; Rosa<sup>nTnG/+</sup>* embryos were

775 stained with anti-GFP antibodies, cleared in BABB, and imaged through the entire

776 pharyngeal region using 25x silicone oil objective N.A. 1.05 and Nikon confocal

777 microscope. 3D reconstruction and surfacing were done using IMARIS. **A.** Pharyngeal

778 mesenchyme in the 1<sup>st</sup> and 2<sup>nd</sup> pharyngeal arches was surfaced. Dashed line marks the

779 plane of transverse optical section shown in **A1**. GFP<sup>+</sup> cells within the pharyngeal

780 mesenchyme (yellow) were quantified using the spot function in IMARIS in the entire

781 volume marked by the yellow surfaces in **A. B –B4**. Splanchnic mesoderm within the

782 dorsal pericardial wall was surfaced in pink, and pharyngeal mesenchyme was surfaced

783 in yellow. **B.** Ventral view. **B1.** Right-side view. Dashed line indicates the plane of

784 section shown in **B3. B2.** A slanted, sagittal/coronal view to visualize both the

785 splanchnic mesoderm and pharyngeal mesenchyme. **B3.** GFP<sup>+</sup> cells in the splanchnic

786 mesoderm (pink) and in the posterior pharyngeal mesenchyme (yellow) were quantified

787 using the spot function in IMARIS throughout the entire volume shown in **B**.

788

789 **Supplemental Figure 5. Step-wise changes in the configuration of the 4<sup>th</sup> arch**

790 **endothelium on the 10<sup>th</sup> day of mouse embryonic development.** Control embryos

791 were stained using antibody to Pecam1. Endothelial cells in the 4<sup>th</sup> pharyngeal arch

792 were surface-rendered yellow using IMARIS. First row, 30-somite stage. Endothelium in

793 the 4<sup>th</sup> arch is in the form of a plexus of small blood vessels. Second row 33-somite  
794 embryo. A small PAA is seen forming. Red stars mark spaces amidst the  
795 interconnected plexus vessels and the small PAA. Third row, 33-somite stage. A large  
796 PAA is seen with connecting plexus vessels. Spaces (marked by the red stars) are still  
797 seen. Fourth row – 36 – 40 – somite stage. A large PAA is present in the 4<sup>th</sup> arch by the  
798 evening of the 10<sup>th</sup> day. DA – dorsal aorta. PAAs are numbers. All scale bars are 50  $\mu$ m.  
799

800 **Supplemental Figure 6. The expression of integrin  $\alpha 5\beta 1$  in the *Isl1* lineages**

801 **regulates the differentiation of neural crest-derived cells into VSCMs at E11.5**

802 Activation of Notch in the pharyngeal arch mesenchyme is not altered in the mutants.  
803 Coronal section through the pharyngeal regions of Control (**A**) and Mutant (**B**) embryos  
804 were stained to detect green fluorescent protein (GFP, green) marks the *Isl1* lineages;  
805 Notch intracellular domain (NICD, orange) is used as the readout of active Notch  
806 signaling; and a smooth muscle actin ( $\alpha$ SMA, blue) marks smooth muscle cells. PAAs  
807 are numbered. The magnification is the same in all panels.

808

809 **Supplemental Figure 7. PAA formation is not affected when integrin  $\alpha 5$  is ablated**

810 **using *Sox17*<sup>2A-iCre</sup> knock-in strain.** Whole-mount pictures were taken following India

811 Ink injections into the hearts of controls and mutants isolated at E10.5. Magnification is

812 the same in all panels.

813

## 814 References

- 815 1. Stoller JZ and Epstein JA. Cardiac neural crest. *Semin Cell Dev Biol.*  
816 2005;16:704-15.
- 817 2. Schreiber C, Mazzitelli D, Haehnel JC, Lorenz HP and Meisner H. The  
818 interrupted aortic arch: an overview after 20 years of surgical treatment. *Eur J*  
819 *Cardiothorac Surg.* 1997;12:466-9; discussion 469-70.
- 820 3. Kellenberger CJ. Aortic arch malformations. *Pediatr Radiol.* 2010;40:876-84.
- 821 4. Psillas G, Kekes G, Constantinidis J, Triaridis S and Vital V. Subclavian steal  
822 syndrome: neurotological manifestations. *Acta Otorhinolaryngol Ital.* 2007;27:33-7.
- 823 5. Kirby ML. *Cardiac Development.* New York: Oxford University Press; 2007.
- 824 6. Moon A. Mouse models of congenital cardiovascular disease. *Curr Top Dev Biol.*  
825 2008;84:171-248.
- 826 7. Nagelberg D, Wang J, Su R, Torres-Vazquez J, Targoff KL, Poss KD and Knaut  
827 H. Origin, Specification, and Plasticity of the Great Vessels of the Heart. *Curr Biol.*  
828 2015;25:2099-110.
- 829 8. Paffett-Lugassy N, Singh R, Nevis KR, Guner-Ataman B, O'Loughlin E, Jahangiri  
830 L, Harvey RP, Burns CG and Burns CE. Heart field origin of great vessel precursors  
831 relies on nkx2.5-mediated vasculogenesis. *Nat Cell Biol.* 2013;15:1362-9.
- 832 9. Wang X, Chen D, Chen K, Jubran A, Ramirez A and Astrof S. Endothelium in the  
833 pharyngeal arches 3, 4 and 6 is derived from the second heart field. *Dev Biol.*  
834 2017;421:108-117.
- 835 10. Li P, Pashmforoush M and Sucov HM. Mesodermal retinoic acid signaling  
836 regulates endothelial cell coalescence in caudal pharyngeal arch artery vasculogenesis.  
837 *Dev Biol.* 2012;361:116-24.
- 838 11. Bremer JL. The development of the aorta and aortic arches in rabbits. *American*  
839 *Journal of Anatomy.* 1912;13:111-128.
- 840 12. DeRuiter MC, Poelmann RE, Mentink MM, Vaniperen L and Gittenberger-De  
841 Groot AC. Early formation of the vascular system in quail embryos. *Anat Rec.*  
842 1993;235:261-74.

- 843 13. Abrial M, Paffett-Lugassy N, Jeffrey S, Jordan D, O'Loughlin E, Frederick CJ,  
844 3rd, Burns CG and Burns CE. TGF-beta Signaling Is Necessary and Sufficient for  
845 Pharyngeal Arch Artery Angioblast Formation. *Cell Rep.* 2017;20:973-983.
- 846 14. Guner-Ataman B, Paffett-Lugassy N, Adams MS, Nevis KR, Jahangiri L,  
847 Obregon P, Kikuchi K, Poss KD, Burns CE and Burns CG. Zebrafish second heart field  
848 development relies on progenitor specification in anterior lateral plate mesoderm and  
849 nkx2.5 function. *Development.* 2013;140:1353-63.
- 850 15. Guner-Ataman B, Gonzalez-Rosa JM, Shah HN, Butty VL, Jeffrey S, Abrial M,  
851 Boyer LA, Burns CG and Burns CE. Failed Progenitor Specification Underlies the  
852 Cardiopharyngeal Phenotypes in a Zebrafish Model of 22q11.2 Deletion Syndrome. *Cell*  
853 *Rep.* 2018;24:1342-1354 e5.
- 854 16. Holowiecki A, Linstrum K, Ravisankar P, Chetal K, Salomonis N and Waxman  
855 JS. Pbx4 limits heart size and fosters arch artery formation through partitioning second  
856 heart field progenitors and restricting proliferation. *Development.* 2020.
- 857 17. Gittenberger-de Groot AC, DeRuiter MC, Bergwerff M and Poelmann RE.  
858 Smooth muscle cell origin and its relation to heterogeneity in development and disease.  
859 *Arterioscler Thromb Vasc Biol.* 1999;19:1589-94.
- 860 18. Bockman DE, Redmond ME, Waldo K, Davis H and Kirby ML. Effect of neural  
861 crest ablation on development of the heart and arch arteries in the chick. *The American*  
862 *journal of anatomy.* 1987;180:332-41.
- 863 19. Hutson MR and Kirby ML. Model systems for the study of heart development and  
864 disease. Cardiac neural crest and conotruncal malformations. *Semin Cell Dev Biol.*  
865 2007;18:101-10.
- 866 20. Hutson MR, Sackey FN, Lunney K and Kirby ML. Blocking hedgehog signaling  
867 after ablation of the dorsal neural tube allows regeneration of the cardiac neural crest  
868 and rescue of outflow tract septation. *Dev Biol.* 2009;335:367-73.
- 869 21. Rosenquist TH, Kirby ML and van Mierop LH. Solitary aortic arch artery. A result  
870 of surgical ablation of cardiac neural crest and nodose placode in the avian embryo.  
871 *Circulation.* 1989;80:1469-75.
- 872 22. Keyte A and Hutson MR. The neural crest in cardiac congenital anomalies.  
873 *Differentiation; research in biological diversity.* 2012;84:25-40.
- 874 23. Coles EG, Gammill LS, Miner JH and Bronner-Fraser M. Abnormalities in neural  
875 crest cell migration in laminin alpha5 mutant mice. *Dev Biol.* 2006;289:218-28.

- 876 24. Cooley MA, Kern CB, Fresco VM, Wessels A, Thompson RP, McQuinn TC, Twal  
877 WO, Mjaatvedt CH, Drake CJ and Argraves WS. Fibulin-1 is required for  
878 morphogenesis of neural crest-derived structures. *Dev Biol.* 2008;319:336-45.
- 879 25. Rydeen AB and Waxman JS. Cyp26 Enzymes Facilitate Second Heart Field  
880 Progenitor Addition and Maintenance of Ventricular Integrity. *PLoS Biol.*  
881 2016;14:e2000504.
- 882 26. Wickstrom SA, Radovanac K and Fassler R. Genetic analyses of integrin  
883 signaling. *Cold Spring Harb Perspect Biol.* 2011;3.
- 884 27. Astrof S. Interactions between neural crest-derived cells and extracellular  
885 microenvironment during cardiovascular development. In: D. W. Desimone and R. P.  
886 Mecham, eds. *Extracellular Matrix in Development* Berlin: Springer Verlag; 2013: 105-  
887 131.
- 888 28. Mittal A, Pulina M, Hou SY and Astrof S. Fibronectin and integrin alpha 5 play  
889 essential roles in the development of the cardiac neural crest. *Mech Dev.* 2010;127:472-  
890 84.
- 891 29. Chen D, Wang X, Liang D, Gordon J, Mittal A, Manley N, Degenhardt K and  
892 Astrof S. Fibronectin signals through integrin alpha5beta1 to regulate cardiovascular  
893 development in a cell type-specific manner. *Dev Biol.* 2015;407:195-210.
- 894 30. Wang X and Astrof S. Isolation of Mouse Cardiac Neural Crest Cells and Their  
895 Differentiation into Smooth Muscle Cells. *Bio Protoc.* 2017;7.
- 896 31. Wang X and Astrof S. Neural crest cell-autonomous roles of fibronectin in  
897 cardiovascular development. *Development.* 2016;143:88-100.
- 898 32. Humphries JD, Byron A and Humphries MJ. Integrin ligands at a glance. *J Cell*  
899 *Sci.* 2006;119:3901-3.
- 900 33. Hynes RO and Naba A. Overview of the matrisome--an inventory of extracellular  
901 matrix constituents and functions. *Cold Spring Harbor perspectives in biology.*  
902 2012;4:a004903.
- 903 34. Pulina M, Liang D and Astrof S. Shape and position of the node and notochord  
904 along the bilateral plane of symmetry are regulated by cell-extracellular matrix  
905 interactions. *Biology open.* 2014;3:583-90.



- 906 35. George EL, Baldwin HS and Hynes RO. Fibronectins are essential for heart and  
907 blood vessel morphogenesis but are dispensable for initial specification of precursor  
908 cells. *Blood*. 1997;90:3073-81.
- 909 36. George EL, Georges-Labouesse EN, Patel-King RS, Rayburn H and Hynes RO.  
910 Defects in mesoderm, neural tube and vascular development in mouse embryos lacking  
911 fibronectin. *Development*. 1993;119:1079-91.
- 912 37. Georges-Labouesse EN, George EL, Rayburn H and Hynes RO. Mesodermal  
913 development in mouse embryos mutant for fibronectin. *Dev Dyn*. 1996;207:145-56.
- 914 38. Pulina MV, Hou SY, Mittal A, Julich D, Whittaker CA, Holley SA, Hynes RO and  
915 Astrof S. Essential roles of fibronectin in the development of the left-right embryonic  
916 body plan. *Dev Biol*. 2011;354:208-20.
- 917 39. Yang JT, Bader BL, Kreidberg JA, Ullman-Cullere M, Trevithick JE and Hynes  
918 RO. Overlapping and independent functions of fibronectin receptor integrins in early  
919 mesodermal development. *Dev Biol*. 1999;215:264-77.
- 920 40. Yang JT, Rayburn H and Hynes RO. Embryonic mesodermal defects in alpha 5  
921 integrin-deficient mice. *Development*. 1993;119:1093-105.
- 922 41. Mittal A, Pulina M, Hou S and Astrof S. Fibronectin and integrin alpha 5 play  
923 requisite roles in cardiac morphogenesis. *Dev Biol*. 2013;381:73-82.
- 924 42. Sun Y, Liang X, Najafi N, Cass M, Lin L, Cai CL, Chen J and Evans SM. Islet 1 is  
925 expressed in distinct cardiovascular lineages, including pacemaker and coronary  
926 vascular cells. *Dev Biol*. 2007;304:286-96.
- 927 43. Devine WP, Wythe JD, George M, Koshiba-Takeuchi K and Bruneau BG. Early  
928 patterning and specification of cardiac progenitors in gastrulating mesoderm. *eLife*.  
929 2014;3.
- 930 44. Ramirez A and Astrof S. Visualization and Analysis of Pharyngeal Arch Arteries  
931 using Whole-mount Immunohistochemistry and 3D Reconstruction. *J Vis Exp*.  
932 2020;157:e60797.
- 933 45. Fish JE, Cantu Gutierrez M, Dang LT, Khyzha N, Chen Z, Veitch S, Cheng HS,  
934 Khor M, Antounians L, Njock MS, Boudreau E, Herman AM, Rhyner AM, Ruiz OE,  
935 Eisenhoffer GT, Medina-Rivera A, Wilson MD and Wythe JD. Dynamic regulation of  
936 VEGF-inducible genes by an ERK/ERG/p300 transcriptional network. *Development*.  
937 2017;144:2428-2444.

- 938 46. Jia G, Preussner J, Chen X, Guenther S, Yuan X, Yekelchik M, Kuenne C,  
939 Looso M, Zhou Y, Teichmann S and Braun T. Single cell RNA-seq and ATAC-seq  
940 analysis of cardiac progenitor cell transition states and lineage settlement. *Nat*  
941 *Commun.* 2018;9:4877.
- 942 47. Verzi MP, McCulley DJ, De Val S, Dodou E and Black BL. The right ventricle,  
943 outflow tract, and ventricular septum comprise a restricted expression domain within the  
944 secondary/anterior heart field. *Dev Biol.* 2005;287:134-45.
- 945 48. Dodou E, Verzi MP, Anderson JP, Xu SM and Black BL. Mef2c is a direct  
946 transcriptional target of ISL1 and GATA factors in the anterior heart field during mouse  
947 embryonic development. *Development.* 2004;131:3931-42.
- 948 49. Papangelis I and Scambler PJ. Tbx1 genetically interacts with the transforming  
949 growth factor-beta/bone morphogenetic protein inhibitor Smad7 during great vessel  
950 remodeling. *Circ Res.* 2013;112:90-102.
- 951 50. Lindsay EA and Baldini A. Recovery from arterial growth delay reduces  
952 penetrance of cardiovascular defects in mice deleted for the DiGeorge syndrome  
953 region. *Human molecular genetics.* 2001;10:997-1002.
- 954 51. Waldo KL, Kumiski D and Kirby ML. Cardiac neural crest is essential for the  
955 persistence rather than the formation of an arch artery. *Dev Dyn.* 1996;205:281-92.
- 956 52. High FA, Zhang M, Proweller A, Tu L, Parmacek MS, Pear WS and Epstein JA.  
957 An essential role for Notch in neural crest during cardiovascular development and  
958 smooth muscle differentiation. *J Clin Invest.* 2007;117:353-63.
- 959 53. High FA, Jain R, Stoller JZ, Antonucci NB, Lu MM, Loomes KM, Kaestner KH,  
960 Pear WS and Epstein JA. Murine Jagged1/Notch signaling in the second heart field  
961 orchestrates Fgf8 expression and tissue-tissue interactions during outflow tract  
962 development. *J Clin Invest.* 2009;119:1986-96.
- 963 54. High FA, Lu MM, Pear WS, Loomes KM, Kaestner KH and Epstein JA.  
964 Endothelial expression of the Notch ligand Jagged1 is required for vascular smooth  
965 muscle development. *Proceedings of the National Academy of Sciences %R*  
966 *101073/pnas0709663105.* 2008;105:1955-1959.
- 967 55. Manderfield LJ, Aghajanian H, Engleka KA, Lim LY, Lui F, Jain R, Li L, Olson EN  
968 and Epstein JA. Hippo signaling is required for Notch-dependent smooth muscle  
969 differentiation of neural crest. *Development.* 2015.

- 970 56. Manderfield LJ, High FA, Engleka KA, Liu F, Li L, Rentschler S and Epstein JA.  
971 Notch activation of Jagged1 contributes to the assembly of the arterial wall. *Circulation*.  
972 2012;125:314-23.
- 973 57. Hellstrom M, Gerhardt H, Kalen M, Li X, Eriksson U, Wolburg H and Betsholtz C.  
974 Lack of pericytes leads to endothelial hyperplasia and abnormal vascular  
975 morphogenesis. *J Cell Biol*. 2001;153:543-53.
- 976 58. Jiang X, Rowitch DH, Soriano P, McMahon AP and Sucov HM. Fate of the  
977 mammalian cardiac neural crest. *Development*. 2000;127:1607-1616.
- 978 59. Liang D, Wang X, Mittal A, Dhiman S, Hou SY, Degenhardt K and Astrof S.  
979 Mesodermal expression of integrin alpha5beta1 regulates neural crest development and  
980 cardiovascular morphogenesis. *Dev Biol*. 2014;395:232–244.
- 981 60. Engleka KA, Manderfield LJ, Brust RD, Li L, Cohen A, Dymecki SM and Epstein  
982 JA. Islet1 derivatives in the heart are of both neural crest and second heart field origin.  
983 *Circ Res*. 2012;110:922-6.
- 984 61. van der Flier A, Badu-Nkansah K, Whittaker CA, Crowley D, Bronson RT, Lacy-  
985 Hulbert A and Hynes RO. Endothelial alpha5 and alphav integrins cooperate in  
986 remodeling of the vasculature during development. *Development*. 2010;137:2439-49.
- 987 62. Engert S, Liao WP, Burtscher I and Lickert H. Sox17-2A-iCre: a knock-in mouse  
988 line expressing Cre recombinase in endoderm and vascular endothelial cells. *Genesis*.  
989 2009;47:603-10.
- 990 63. Calmont A, Ivins S, Van Bueren KL, Papangelis I, Kyriakopoulou V, Andrews WD,  
991 Martin JF, Moon AM, Illingworth EA, Basson MA and Scambler PJ. Tbx1 controls  
992 cardiac neural crest cell migration during arch artery development by regulating Gbx2  
993 expression in the pharyngeal ectoderm. *Development*. 2009;136:3173-83.
- 994 64. Gitler AD, Lu MM and Epstein JA. PlexinD1 and semaphorin signaling are  
995 required in endothelial cells for cardiovascular development. *Dev Cell*. 2004;7:107-16.
- 996 65. Merscher S, Funke B, Epstein JA, Heyer J, Puech A, Lu MM, Xavier RJ, Demay  
997 MB, Russell RG, Factor S, Tokooya K, Jore BS, Lopez M, Pandita RK, Lia M, Carrion  
998 D, Xu H, Schorle H, Kobler JB, Scambler P, Wynshaw-Boris A, Skoultchi AI, Morrow BE  
999 and Kucherlapati R. TBX1 is responsible for cardiovascular defects in velo-cardio-  
1000 facial/DiGeorge syndrome. *Cell*. 2001;104:619-29.
- 1001 66. Phillips HM, Stothard CA, Shaikh Qureshi WM, Kousa AI, Briones-Leon JA,  
1002 Khasawneh RR, O'Loughlin C, Sanders R, Mazzotta S, Dodds R, Seidel K, Bates T,

- 1003 Nakatomi M, Cockell SJ, Schneider JE, Mohun TJ, Maehr R, Kist R, Peters H and  
1004 Bamforth SD. Pax9 is required for cardiovascular development and interacts with Tbx1  
1005 in the pharyngeal endoderm to control 4th pharyngeal arch artery morphogenesis.  
1006 *Development*. 2019;146.
- 1007 67. Macatee TL, Hammond BP, Arenkiel BR, Francis L, Frank DU and Moon AM.  
1008 Ablation of specific expression domains reveals discrete functions of ectoderm- and  
1009 endoderm-derived FGF8 during cardiovascular and pharyngeal development.  
1010 *Development*. 2003;130:6361-74.
- 1011 68. Cai CL, Liang X, Shi Y, Chu PH, Pfaff SL, Chen J and Evans S. Isl1 identifies a  
1012 cardiac progenitor population that proliferates prior to differentiation and contributes a  
1013 majority of cells to the heart. *Dev Cell*. 2003;5:877-89.
- 1014 69. Baldini A, Fulcoli FG and Illingworth E. Tbx1: Transcriptional and Developmental  
1015 Functions. *Current topics in developmental biology*. 2017;122:223-243.
- 1016 70. Graham A, Okabe M and Quinlan R. The role of the endoderm in the  
1017 development and evolution of the pharyngeal arches. *J Anat*. 2005;207:479-87.
- 1018 71. Alfano D, Altomonte A, Cortes C, Bilio M, Kelly RG and Baldini A. Tbx1 regulates  
1019 extracellular matrix-cell interactions in the second heart field. *Human molecular  
1020 genetics*. 2019;28:2295-2308.
- 1021 72. Francou A, Saint-Michel E, Mesbah K and Kelly RG. TBX1 regulates epithelial  
1022 polarity and dynamic basal filopodia in the second heart field. *Development*.  
1023 2014;141:4320-31.
- 1024 73. van Bueren KL, Papangelis I, Rochais F, Pearce K, Roberts C, Calmont A,  
1025 Szumska D, Kelly RG, Bhattacharya S and Scambler PJ. Hes1 expression is reduced in  
1026 Tbx1 null cells and is required for the development of structures affected in 22q11  
1027 deletion syndrome. *Dev Biol*. 2010;340:369-80.
- 1028 74. Aghajanian H, Choi C, Ho VC, Gupta M, Singh MK and Epstein JA. Semaphorin  
1029 3d and semaphorin 3e direct endothelial motility through distinct molecular signaling  
1030 pathways. *J Biol Chem*. 2014;289:17971-9.
- 1031 75. Cohen ED, Wang Z, Lepore JJ, Lu MM, Taketo MM, Epstein DJ and Morrissey  
1032 EE. Wnt/beta-catenin signaling promotes expansion of Isl-1-positive cardiac progenitor  
1033 cells through regulation of FGF signaling. *J Clin Invest*. 2007;117:1794-804.
- 1034 76. Degenhardt K, Singh MK, Aghajanian H, Massera D, Wang Q, Li J, Li L, Choi C,  
1035 Yzaguirre AD, Francey LJ, Gallant E, Krantz ID, Gruber PJ and Epstein JA. Semaphorin

- 1036 3d signaling defects are associated with anomalous pulmonary venous connections.  
1037 *Nat Med.* 2013;19:760-5.
- 1038 77. Frank DU, Fotheringham LK, Brewer JA, Muglia LJ, Tristani-Firouzi M, Capecchi  
1039 MR and Moon AM. An *Fgf8* mouse mutant phenocopies human 22q11 deletion  
1040 syndrome. *Development.* 2002;129:4591-603.
- 1041 78. Park EJ, Ogden LA, Talbot A, Evans S, Cai CL, Black BL, Frank DU and Moon  
1042 AM. Required, tissue-specific roles for *Fgf8* in outflow tract formation and remodeling.  
1043 *Development.* 2006;133:2419-33.
- 1044 79. Park EJ, Watanabe Y, Smyth G, Miyagawa-Tomita S, Meyers E, Klingensmith J,  
1045 Camenisch T, Buckingham M and Moon AM. An FGF autocrine loop initiated in second  
1046 heart field mesoderm regulates morphogenesis at the arterial pole of the heart.  
1047 *Development.* 2008;135:3599-610.
- 1048 80. Watanabe Y, Miyagawa-Tomita S, Vincent SD, Kelly RG, Moon AM and  
1049 Buckingham ME. Role of mesodermal FGF8 and FGF10 overlaps in the development of  
1050 the arterial pole of the heart and pharyngeal arch arteries. *Circ Res.* 2010;106:495-503.
- 1051 81. Stalmans I, Lambrechts D, De Smet F, Jansen S, Wang J, Maity S, Kneer P, von  
1052 der Ohe M, Swillen A, Maes C, Gewillig M, Molin DG, Hellings P, Boetel T, Haardt M,  
1053 Compennolle V, Dewerchin M, Plaisance S, Vlietinck R, Emanuel B, Gittenberger-de  
1054 Groot AC, Scambler P, Morrow B, Driscoll DA, Moons L, Esguerra CV, Carmeliet G,  
1055 Behn-Krappa A, Devriendt K, Collen D, Conway SJ and Carmeliet P. VEGF: a modifier  
1056 of the del22q11 (DiGeorge) syndrome? *Nat Med.* 2003;9:173-82.
- 1057 82. Oh J, Richardson JA and Olson EN. Requirement of myocardin-related  
1058 transcription factor-B for remodeling of branchial arch arteries and smooth muscle  
1059 differentiation. *Proc Natl Acad Sci U S A.* 2005;102:15122-7.
- 1060 83. Hellstrom M, Kalen M, Lindahl P, Abramsson A and Betsholtz C. Role of PDGF-B  
1061 and PDGFR-beta in recruitment of vascular smooth muscle cells and pericytes during  
1062 embryonic blood vessel formation in the mouse. *Development.* 1999;126:3047-55.
- 1063 84. Scambler PJ. The 22q11 deletion syndromes. *Human molecular genetics.*  
1064 2000;9:2421-6.
- 1065 85. Momma K. Cardiovascular anomalies associated with chromosome 22q11.2  
1066 deletion syndrome. *Am J Cardiol.* 2010;105:1617-24.
- 1067 86. Lindsay EA, Vitelli F, Su H, Morishima M, Huynh T, Pramparo T, Jurecic V,  
1068 Ogunrinu G, Sutherland HF, Scambler PJ, Bradley A and Baldini A. *Tbx1*

1069 haploinsufficiency in the DiGeorge syndrome region causes aortic arch defects in mice.  
1070 *Nature*. 2001;410:97-101.

1071 87. Jerome LA and Papaioannou VE. DiGeorge syndrome phenotype in mice mutant  
1072 for the T-box gene, Tbx1. *Nat Genet*. 2001;27:286-91.

1073

# FIGURE 1

MEF2C-AHF-DreERT2 Tamoxifen injection at E8.0

VEGFR2 tdTomato

VEGFR2 tdTomato

VEGFR2 ERG

**Figure 1. Endothelial PAA progenitors are present in the second heart field as early as E7.25.** *Isl1<sup>MerCreMer</sup>* and *Mef2C-AHF-DreERT2* males were mated with the appropriate reporter females (see Methods). E0.5 was considered to be noon on the day of the vaginal plug. Tamoxifen was injected at specified times, embryos were dissected at E10.5, and stained to detect VEGFR2 (blue), ERG (red), or tdTomato (orange).

**A.** Sagittal view and 3D reconstruction through the left pharyngeal region. Inset- 3D reconstruction of PAAs. **A1 – A2.** Sagittal optical sections through the embryo shown in **A**. Labeling efficiency was quantified by calculating the ratio of the number of ERG<sup>+</sup> tdTomato<sup>+</sup> ECs to the total number of ERG<sup>+</sup> ECs in PAAs using IMARIS spot function. **B.** Highest labeling of PAA endothelium occurred when tamoxifen was injected at E7.25 in *Isl1<sup>MerCreMer</sup>* knockin mice. **B1.** SHF-derived cells continue to be added the 4<sup>th</sup> PAA after E9.5. **C.** Peak labeling of PAA ECs occurred when tamoxifen was injected at E8.0 in *Mef2C-AHF-DreERT2* strain. **C1.** Injection of tamoxifen at E8.5 led to a more efficient labeling of the 4<sup>th</sup> PAAs than the 3<sup>rd</sup> and 6<sup>th</sup> PAAs.

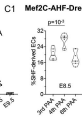
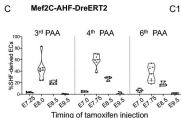
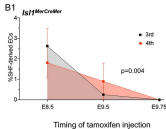
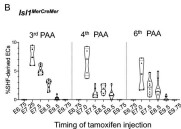
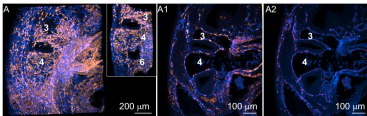


**FIGURE 2**

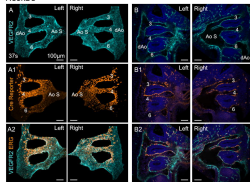
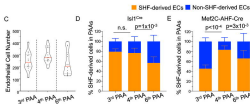
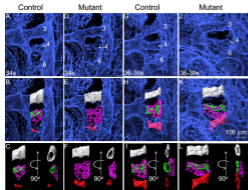


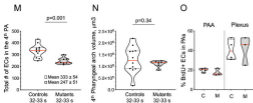
Figure 2. Majority of PAA ECs are SHF-derived; there are differences in the contribution of the SHF to the PAA endothelium depending on the strain used. *Mei2C-AHF-Cre; ROSA<sup>lTomato</sup>* embryos (35 – 37 somites) were stained with antibodies to VEGFR2 (turquoise) to detect endothelial cells, *IdTomato* (orange) to detect SHF-derived cells, and DAPI (blue) to stain cell nuclei. **A – A2.** 3D reconstructions of PAAs and their connections with the dorsal aorta (dAo) and the aortic sac (Ao S). **B – B2.** Sagittal optical sections to show the distribution of all SHF-derived cells in the pharyngeal arches. PAAs 3 – 5 are labeled. Magnifications are the same in all panels. All scale bars are 100  $\mu$ m. **C.** The number of VEGFR2<sup>+</sup>EGR<sup>+</sup> cells in the pharyngeal arches was quantified in 5 E10.5 embryos at 35 – 37 somites using IMARIS. Each dot is one arch. Red line marks the median. Black lines mark quartiles. Differences among the three PAA pairs are not significant,  $p > 0.1$  by one-way ANOVA with Tukey's correction for multiple testing. **D – E.** The percentage of VEGFR2<sup>+</sup>EGR<sup>+</sup> cells expressing the Cre reporter was determined in each PAA (orange bars). Blue bars are the percent of VEGFR2<sup>+</sup>EGR<sup>+</sup> cells that were not labeled with the Cre reporter. **D.** The use of constitutive *Isl1<sup>Cre</sup>* strain resulted in labeling of more than 80% of ECs in the 3<sup>rd</sup> and 4<sup>th</sup> PAAs. **E.** The use of *Mei2C-AHF-Cre* strain resulted in a significantly higher labeling of the 4<sup>th</sup> PAAs than the 3<sup>rd</sup> and the 6<sup>th</sup>. The difference in the labeling efficiency of 6<sup>th</sup> PAAs between the two strains was not significant,  $p > 0.2$ . All statistical analyses were performed using one-way ANOVA with Tukey's correction for multiple testing.

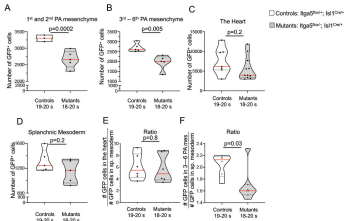




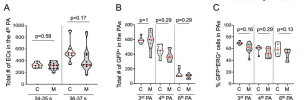
**FIGURE 3**

**Figure 3. Formation of the 4<sup>th</sup> PAA is delayed in integrin  $\alpha 5^{lox/-}; Isl1^{Cre}$  mutants.**  $\alpha 5^{lox/-}; Isl1^{Cre}$  control and  $\alpha 5^{lox/-}; Isl1^{Cre}$  mutant embryos were dissected at different somite stages at E10.5 and stained to detect Pecam1. PAAs are numbered and somite stages are indicated in the first row. **A, D, G, J.** 3D reconstructions of whole-mount Pecam 1 staining (light blue). **B, E, H, K.** PAA endothelium in the 3<sup>rd</sup>, 4<sup>th</sup> and 6<sup>th</sup> arches shown in the row above was surface-rendered white, green and red, respectively. In addition, the plexus endothelium in the 4<sup>th</sup> arch was surface-rendered in pink. **C, F, I, L.** Left side and ventral views of surface-rendered PAAs and the plexus. Development of the 4<sup>th</sup> PAAs was specifically affected in the mutants (**E, F**). Magnification is the same in all panels. Scale bar is 100  $\mu$ m. **M.** Total number of endothelial cells was quantified as described in Methods. Mutants have EC deficiency in the 4<sup>th</sup> arch as 32 – 33 somites. **N.** The sizes of the 4<sup>th</sup> arches are comparable between controls and mutants. **O.** EC proliferation in the PAA and plexus in the 4<sup>th</sup> arches was similar in controls (**C**) and mutants (**M**). In all plots, solid lines mark the median, dashed lines mark the quartiles. Each dot marks one arch. At least 3 mutants and 3 controls were assayed. Statistics were evaluated using 2-tailed, unpaired Student's *t* test with Welch's correction for unequal standard deviation between samples.

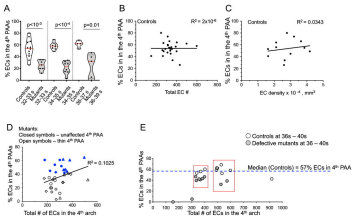


**FIGURE 4**

**Figure 4. The expression of integrin  $\alpha 5$  in the *Isl1* lineages is required for the accrual of SHF-derived cells to the pharyngeal mesenchyme.** Control and mutant embryos carrying one ROSA<sup>trG</sup> reporter allele were dissected at E9.5 (18 – 20 somite stage) and stained with DAPI and anti-GFP antibodies. Whole embryos were imaged and the number of GFP<sup>+</sup> cells (SHF-derivatives) in the arch mesenchyme, splanchnic mesoderm, and in the heart was quantified as described in Sup. Fig. 4. **A**, The total number of SHF cells in the mesenchyme of the 1<sup>st</sup> and 2<sup>nd</sup> arches was decreased in the mutants. **B**, The total number of GFP<sup>+</sup> cells in the pharyngeal mesenchyme corresponding with the future arches 3 – 6 was decreased in the mutants. The number of SHF cells in heart (**C**) and the splanchnic mesoderm (**D**) was not affected. **E**, The proportion of GFP<sup>+</sup> cells in the heart relative to GFP<sup>+</sup> cells in splanchnic mesoderm was not affected in the mutants. **F**, The proportion of GFP<sup>+</sup> cells in the posterior pharyngeal mesenchyme relative to the number of GFP<sup>+</sup> cells in splanchnic mesoderm was significantly decreased in the mutants. Each dot marks one embryo, red lines mark medians, dotted lines mark quartiles; p values were determined using unpaired, 2-tailed Student's t tests.

**FIGURE 5**

**Figure 5. Recovery of EC numbers in integrin  $\alpha 5^{flxed}; Isl1^{Cre+}$  mutants.** **A.** Total EC number has recovered in integrin  $\alpha 5^{flxed}; Isl1^{Cre+}$  mutants by the 34<sup>th</sup> somite stage. **B.** Total number of SHF-derived mesodermal cells has recovered in the pharyngeal arches in integrin  $\alpha 5^{flxed}; Isl1^{Cre+}$  mutants by the 34<sup>th</sup> somite stage. **C.** The fraction of SHF-derived ECs in pharyngeal arches is comparable among control and mutant embryos. This fraction was calculated by quantifying the number of GFP<sup>+</sup>ERG<sup>+</sup> cells and dividing by the total number of ERG<sup>+</sup> cells in the entire pharyngeal arches (e.g. ECs in PAA and plexus were quantified). Statistical significance was evaluated using one-way ANOVA with Tukey's correction for multiple testing.

**FIGURE 6**

**Figure 6. Integrin  $\alpha 5 \beta 1$  and Fn1 regulate the remodeling of EC plexus during the formation of the 4<sup>th</sup> pharyngeal arch arteries.** **A.** The proportion of ECs in the 4<sup>th</sup> PAAs in the mutant is significantly lower than in controls at all stages analyzed at E10.5, including the stages when the EC population in the 4<sup>th</sup> pharyngeal arch has recovered in the mutants; 2-tailed, unpaired Student's t test. **B – C.** Linear regression analyses indicate the absence of linear correlation between the size of the 4<sup>th</sup> PAA and EC number (**B**) or density (**C**). PAA size is expressed as the percentage of pharyngeal arch endothelial cells in the 4<sup>th</sup> PAA in control embryos on the y-axis. **D.** Total EC number (x-axis) from mutants with defective (open symbols) or unaffected 4<sup>th</sup> PAA (closed symbols) were plotted against the size of the 4<sup>th</sup> PAAs, y-axis. Regression analysis indicated low correlation between these properties. Circles: 32 – 33 somite embryos, rhombi: 34 – 35 somite embryos, triangles: 36 – 39 somite embryos. **E.** The rearrangement of the endothelial plexus into the 4<sup>th</sup> PAAs is defective in mutants relative to controls with the same number of endothelial cells in the 4<sup>th</sup> arch (red boxes). EC – endothelial cell(s). Controls:  $\alpha 5 \beta 1$ ; *Isl1*<sup>Cre/+</sup> and *Fn1*<sup>+/+</sup>; *Isl1*<sup>Cre/+</sup> embryos; Mutants:  $\alpha 5 \beta 1$ ; *Isl1*<sup>Cre/+</sup> and *Fn1*<sup>-/-</sup>; *Isl1*<sup>Cre/+</sup> embryos.

# FIGURE 7

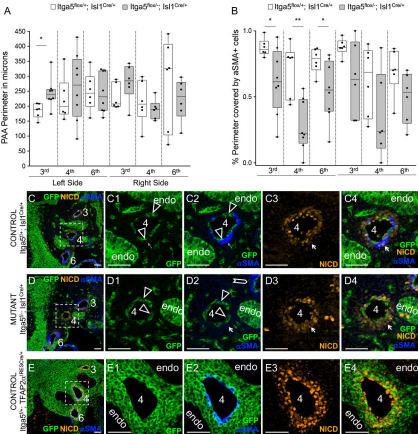


**Figure 7. The expression of integrin  $\alpha 5\beta 1$  in the *Isl1* lineages regulates the differentiation of neural crest-derived cells into VSCMs at E11.5. **A.** PAA perimeter has recovered in size in the mutants by E11.5. **B.** Smooth muscle coverage of the left 4<sup>th</sup> and left 6<sup>th</sup> PAA was deficient in the mutants. **C – D.** Despite defective differentiation of NC cells into VSCMs, the activation of Notch in the pharyngeal arch mesenchyme was not altered in the mutants. PAAs are numbered. PAA ECs at E11.5 are derived from the *Isl1<sup>Cre</sup>* lineage (green, arrowheads in **C1**, **C2** and **D1**, **D2**). **C2 – D2.** VSMC differentiation assayed by the expression of alpha smooth muscle actin ( $\alpha$ SMA, blue) is specifically affected around the 4<sup>th</sup> PAAs in the mutants (compare regions marked by the arrows in **C2** and **D2**). The activation of Notch assayed by the expression of NICD is not altered in the mutants with defective VSMC differentiation (arrows in **C3**, **C4** and **D3**, **D4**). **E.** Fate map using *TFAP2 $\alpha$ <sup>RESOCre</sup>* shows the location of NC-derived cells in the pharyngeal arches. Note extensive colonization of the mesenchyme between the endodermal pouches (endo) by the *TFAP2 $\alpha$ <sup>RESOCre</sup>* lineage.  $\alpha$ SMA<sup>+</sup> cells are GFP-negative in *Isl1Cre* strain (arrows in **C1**–**C2**). **E2.**  $\alpha$ SMA<sup>+</sup> cells are GFP+ in *TFAP2 $\alpha$ <sup>RESOCre</sup>* strain. All scale bars are 50  $\mu$ m. Additional zoom-out views are in Sup. Fig. 6.**

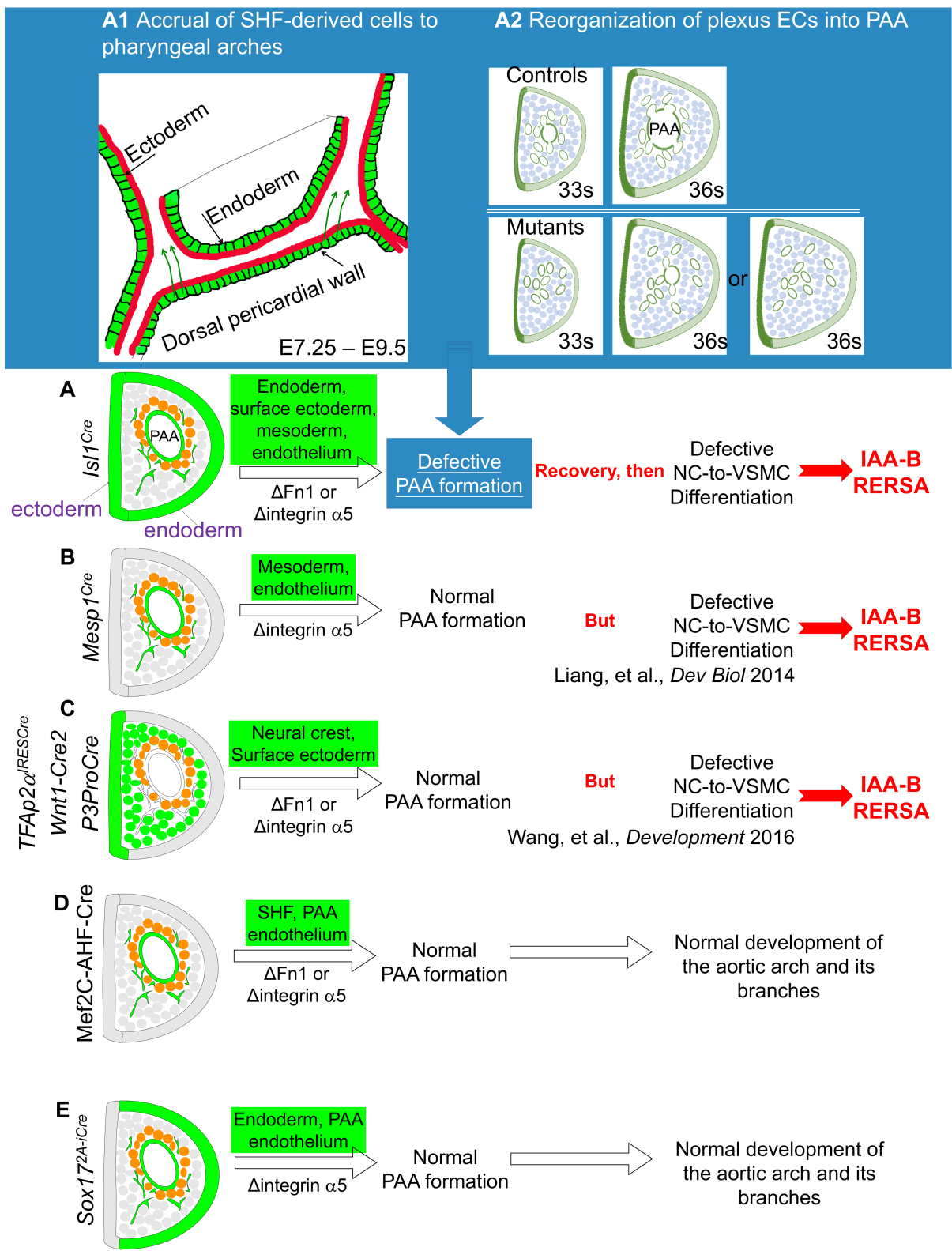


**Figure 8. Cell – ECM interactions play essential roles at multiple stages during the development of the aortic arch and its branches. A – E.** Depictions of coronal sections through the 4<sup>th</sup> pharyngeal arch at E10.5. Lineages are marked in green, NC-derived cells are depicted as circles, NC-derived cells next to the PAA endothelium are marked in orange. **A.** The expression of integrin  $\alpha 5\beta 1$  and Fn1 in the *Isl1* lineages is required for the formation of the 4<sup>th</sup> PAAs (see **A1** and **A2** in the blue inset) as well as for NC-to-VSMC differentiation. The deletion of integrin  $\alpha 5$  or Fn1 in the *Isl1* lineages leads to IAA-B and RERSA. **A1 – A2.** Stages during which integrin  $\alpha 5$  and Fn1 regulate the 4<sup>th</sup> PAA formation. **A1.** A schematic of *Isl1* lineages (green) in the pharynx at E8.5 – E9.5. Green arrows indicate migration of splanchnic mesoderm cells into the pharyngeal arches. Red lines signify enriched localization of Fn1 protein at germ layer borders. Integrin  $\alpha 5\beta 1$  is expressed in all cell types in the pharynx at E8.5 (Chen et al., 2015) and regulates the accrual of pharyngeal mesoderm from the SHF (green arrows). **A2.** During the 10<sup>th</sup> day of mouse development, integrin  $\alpha 5\beta 1$  and Fn1 regulate the remodeling of the plexus endothelium in the 4<sup>th</sup> pharyngeal arch into the PAA. *Isl1* lineages are marked in green. NC-derived cells are in blue. **B.** The expression of integrin  $\alpha 5$  in the mesoderm regulates the differentiation of NC-derived cells into VSMCs. The deletion of integrin  $\alpha 5$  in *Mesp1* lineage, which includes the SHF, leads to defective NC-to-VSMC differentiation and results in the regression of the 4<sup>th</sup> PAAs leading to IAA-B and RERSA (Liang, et al., *Dev Biol* 2014). **C.** Fn1 becomes upregulated in NC-derived cells adjacent to the 4<sup>th</sup> PAA ECs between E10.5 and E11.5. The expression of integrin  $\alpha 5\beta 1$  and Fn1 in the NC-derived cells is required for NC-to-VSMC differentiation and the stability of the 4<sup>th</sup> PAA (Wang et al, 2016). The deletion of either integrin  $\alpha 5$  or Fn1 in the NC (and the surface ectoderm) leads to IAA-B and RERSA but does not impair PAA formation. **D.** The expression integrin  $\alpha 5$  or Fn1 in the SHF is not required for the morphogenesis of the aortic arch and its branches. **E.** The expression of integrin  $\alpha 5$  in the endoderm and the pharyngeal endothelia is not required for the development of the aortic arch and its branches.

bioRxiv preprint doi: <https://doi.org/10.1101/2020.04.07.029926>; this version posted September 18, 2020. The copyright holder for this preprint (which was not certified by peer review) is the author/funder, who has granted bioRxiv a license to display the preprint in perpetuity. It is made available under aCC-BY-NC-ND 4.0 International license.